Neurobiology of Disease 216 (2025) 107113

Contents lists available at ScienceDirect

Neurobiology of Disease

journal homepage: www.elsevier.com/locate/ynbdi

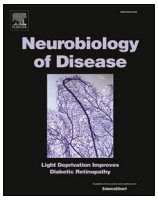

PKR-driven ISR signaling controls synaptic translation and structural plasticity in an age-dependent manner

Nicolás W. Martínez [a,b,1], Felipe Gómez [c,1], Ariel Tapia-Godoy [a], Juan Francisco Roa [a,b], Fernanda Moreso-Contreras [a,c], Yuwei Liu [e], Claudia Jara [a,b], Cheril Tapia-Rojas [a,b], Iván Alfaro [a,d], Mauro Costa-Mattioli [e,f], Soledad Matus [a,b,c,*]

[a] Centro Ciencia & Vida, Fundación Ciencia & Vida, Santiago, 8580702, Chile
[b] Facultad de Ciencias, Universidad San Sebastián, Santiago, 8580704, Chile
[c] Fundación Ciencia & Vida (FCV), Santiago, 8580702, Chile
[d] Programa de Comunicación Celular en Cáncer, Instituto de Ciencias e Innovación en Medicina, Facultad de Medicina, Clínica Alemana, Universidad del Desarrollo, Santiago, 7590943, Chile
[e] Altos Labs, Inc, Bay Area Institute of Science, Redwood City, CA 94065, USA
[f] Department of Neuroscience, Baylor College of Medicine, Houston, TX 77030, USA

ARTICLE INFO

Keywords:
PKR
eIF2α
PSD95
Synapsin
Proteostasis
Neurons

ABSTRACT

The integrated stress response (ISR) modulates protein homeostasis in response to both intracellular and extracellular signals. The four kinases involved in the ISR all phosphorylate the same target, the alpha subunit of eukaryotic initiation factor 2 (eIF2α), to integrate various stress signals, thereby regulating cell fate. The activation of the ISR reprograms the proteome by inhibiting general protein synthesis while increasing the translation of specific mRNAs. In the brain, the ISR regulates the type of synaptic plasticity necessary for forming long-term memory. More importantly, the activation of the ISR has emerged as a causal mechanism underlying cognitive decline associated with a wide range of neurological disorders, prompting several pharmaceutical companies to target the ISR to promote brain health. However, whether the ISR acts at specific localities within neurons, including synapses, remains unclear. Here, we examined the presence, activity, and spatial arrangement of the ISR branch driven by the double-stranded RNA-dependent protein kinase (PKR) (PKR-eIF2α axis) in synapses and assessed the role of PKR in maintaining synaptic proteostasis over time. Our findings demonstrate that both PKR and eIF2α are localized at synapses, where a dynamic PKR-eIF2α axis regulates synaptic size and the abundance of synaptic proteins in an age-dependent manner. Moreover, PKR deficiency leads to an increase in protein synthesis in synapse-enriched fractions. Thus, the PKR branch of the ISR serves as a new regulator of synaptic structural plasticity.

1. Introduction

The integrated stress response (ISR) is a pathway that restores the protein homeostasis (proteostasis) (Costa-Mattioli and Walter, 2020; Wek et al., 2006) by reprogramming gene expression. This reprogramming of the proteome restores the cell's balance and promotes cell and organismal health (Costa-Mattioli and Walter, 2020; Wek et al., 2006). Different stress conditions, including protein folding defects, nutrient deprivation, viral infection, and oxidative stress, are sensed by four specialized kinases: double-stranded RNA-dependent Protein Kinase (PKR), PKR-like ER kinase (PERK), Heme-Regulated eIF2α kinase (HRI) and General Control Non-derepressible 2 (GCN2). These kinases transduce the dynamics of intracellular variables by phosphorylating a common target: the α subunit of the eukaryotic translation initiation factor 2 (eIF2α) (Wek, 2018). The phosphorylation of eIF2α leads to a decrease in general protein synthesis and an increase in the translation of a subset of mRNAs containing upstream open reading frames (uORFs) in their 5′ untranslated regions (UTR) (Hinnebusch, 2005; Lu et al., 2004; Vattem and Wek, 2004). Some of these mRNAs directly regulate gene expression (Hinnebusch, 2005; Lu et al., 2004; Vattem and Wek,

* Corresponding author at: Universidad San Sebastián, Santiago, 8580704, Chile.
E-mail addresses: smatus@cienciavida.org, maria.matus@uss.cl (S. Matus).
[1] These authors contributed equally to this work.

https://doi.org/10.1016/j.nbd.2025.107113
Received 9 June 2025; Received in revised form 15 September 2025; Accepted 17 September 2025
Available online 19 September 2025

2004), like the one encoding the activation transcription factor 4 (ATF4) (Harding et al., 2000), which is the best-characterized downstream effector of the ISR.

In the brain, the ISR has evolved to control the protein synthesis-dependent synaptic plasticity that is required to form long-term memory (Costa-Mattioli et al., 2005; Liu et al., 2014; Lourenco et al., 2013; Costa-Mattioli et al., 2007; Hwang et al., 2017; Placzek et al., 2016; Zhu et al., 2011). Most importantly, ISR activation underlies the cognitive decline in a wide range of neurological disorders (Chang et al., 2002; Hoozemans et al., 2007; Smith and Mallucci, 2016; Moon et al., 2018). As a result, the ISR is emerging as a promising avenue to promote brain health in several neurological conditions resulting from the disruption in protein homeostasis. Yet, little is known about the mechanism by which the ISR modulates brain function.

The ISR kinase PKR is a constitutive serine-threonine kinase that is primarily activated directly by double-stranded RNAs (dsRNAs) from viruses or mitochondria (Dey et al., 2005; Garcia et al., 2007; Kim et al., 2018). PKR has been extensively characterized in replicative cells (Zhu et al., 2011; Anderson et al., 2011; He et al., 2013; Romano et al., 1998; Lacor et al., 2007; Deb et al., 2001; Husain et al., 2015; McAllister et al., 2012; Page et al., 2006; Reimer et al., 2018), where it exhibits a homogeneous cytoplasmic distribution (Takizawa et al., 2000). However, Zappa et al. demonstrated that a stimulus that triggers ISR activation also promotes a partial reorganization of PKR's subcellular distribution, transitioning from widespread PKR in the cytoplasm to a clustered form within stress granules (Zappa et al., 2022). Only a few studies have explored PKR behavior in neurons, where the addition of amyloid β (Aβ) to neuronal branches induces PKR-dependent stress granule formation in neural cells (Ramasamy et al., 2025; Baleriola et al., 2014). This evidence suggests that the effects of PKR activity can vary significantly within the same cell, depending on local cellular contexts or compartments, and that clustering may represent one of the patterns. However, the distribution and localization of the ISR pathway components and their regulatory roles in local cellular phenotypes remains unknown, especially in neurons, which are highly compartmentalized cells.

Neurons maintain their morphological and functional integrity by preserving distinct local phenotypes within their somata, axons, and synapses, each characterized by a unique local dynamic proteome (Pertz et al., 2008; Li et al., 2024; Hobson et al., 2022; Giandomenico et al., 2022; Dorrbaum et al., 2018). Local protein synthesis and degradation have been reported in axons and synapses (Sotelo et al., 2014; Tu et al., 2024; Segref and Hoppe, 2009; Steward and Schuman, 2001; Hafner et al., 2019; Spaulding and Burgess, 2017; Jung et al., 2012; Kim and Jung, 2015; Alvarez, 2001; Alvarez et al., 2000; Court and Alvarez, 2005; Court et al., 2008; Upadhya et al., 2006; Hegde et al., 2014; Dong et al., 2008; Gumy et al., 2010; Hegde, 2004). Although the ISR is a key regulator of protein synthesis, its role in maintaining neuronal local proteomes remains largely unexplored. Intriguingly, local increases in the ISR downstream target ATF4 have been documented in axons in response to Aβ oligomers in compartmentalized settings *in vitro (*Baleriola et al., *2014)*. Thus, given that: a) Aβ oligomers activate the PKR-branch of the ISR locally (Baleriola et al., 2014), and b) synaptic processes have a distinctive abundance and translation efficiency of mRNAs containing regulatory uORFs at the 5'UTR (Glock et al., 2021), it is possible that the ISR could modulate its downstream synaptic local targets. However, the presence of ISR kinases, particularly PKR, and their activity in specific neuronal compartments, such as the synapse, have not been explored.

In recent years, accumulating evidence indicates that ISR kinases and their downstream signaling regulate morphological and functional integrity parameters of the CNS (Costa-Mattioli et al., 2005; Liu et al., 2014; Lourenco et al., 2013; Costa-Mattioli et al., 2007; Hwang et al., 2017; Placzek et al., 2016; Zhu et al., 2011). Specifically, sustained eIF2α phosphorylation reduces the pre and postsynaptic numeric densities of hippocampal neurons *in vitro (*Lourenco et al., *2013)* while *knockdown* of the ISR effector ATF4 alters postsynaptic numeric densities *in vitro* and *in vivo (*Liu et al., *2014)*. These findings suggest that non-local modulation of ISR activity can profoundly influence synaptic organization. Interestingly, several modulators of synaptic activity also affect the phosphorylation status of eIF2α in neurons *in vivo* and *in vitro* (Alvarez-Castelao et al., 2020; Biever et al., 2016; Dorrbaum et al., 2020), supporting the idea that activity-driven eIF2α phosphorylation could act as a switch to enhance the local translational efficiency of uORF-containing transcripts encoding key plasticity-related proteins (Glock et al., 2021). This mechanism could directly reshape the synaptic proteome, driving changes in synaptic protein composition. It is consensual that fast and context-specific changes in the abundance and activity of synaptic proteins and the size and strength of synaptic contacts support learning and memory through synaptic phenotype adaptation. These changes that remodel synapses are known as synaptic plasticity and have two forms: long-term potentiation (LTP) and long-term depression (LTD), with specific mechanisms that can be dependent or independent of protein synthesis (Bin Ibrahim et al., 2022; Jedrzejewska-Szmek and Blackwell, 2019; Murai and Goto, 2025; Rajgor et al., 2021). Several studies measuring protein synthesis-dependent synaptic transmission readouts at electrophysiological recordings from hippocampal slices have demonstrated that PKR and eIF2α genetic or pharmacological downregulation modulate transmission efficiency (Costa-Mattioli et al., 2005; Costa-Mattioli et al., 2007; Hwang et al., 2017; Placzek et al., 2016; Zhu et al., 2011; Stern et al., 2013), probably through synaptic local proteomes. Moreover, in those studies, the learning and memory tasks evaluated demonstrate that ISR activity regulates cognition by reducing the amount of experience or training needed to form specific types of memories (Costa-Mattioli et al., 2007).

Local protein synthesis at synapses is essential for the rapid and spatially restricted remodeling of synaptic connections required for plasticity, learning, and memory (Steward and Schuman, 2001; Hafner et al., 2019; Sutton and Schuman, 2006). Synaptically localized mRNAs and translational machinery allow neurons to respond to activity-dependent signals by producing proteins directly at the synapse, allowing fine-tuned regulation of synaptic strength and composition (Glock et al., 2021; Rajgor et al., 2021). While the ISR is a master regulator of protein synthesis, it remains unclear whether it operates directly within synaptic compartments to control local translation. Among the ISR kinases, PKR is particularly interesting because its activation leads to phosphorylation of eIF2α, which globally suppresses translation while selectively enhancing the synthesis of specific uORF-containing mRNAs, some of which are involved in synaptic plasticity (Costa-Mattioli et al., 2005; Costa-Mattioli et al., 2007; Zhu et al., 2011; Glock et al., 2021). This raises the intriguing possibility that PKR could locally influence synaptic proteostasis by controlling translation at the synapse. However, whether PKR and eIF2α are indeed present and active at synapses, or if they modulate proteomic changes needed for excitability modulation, remains unexplored.

It has been widely demonstrated that synaptic morphology and functional integrity decline during aging (Azpurua and Eaton, 2015; Barrantes, 2024; Cicali and Tapia-Rojas, 2024; Fan et al., 2018; Navakkode and Kennedy, 2024; Petralia et al., 2014). Additionally, it has been established that aging synapses have a distinctive dynamic proteomic composition compared to young brain structures, such as in the cortex and hippocampus (VanGuilder et al., 2010; Vegh et al., 2014). In this context, notorious dysfunctional changes in synaptic proteins that promote synaptic plasticity have been observed during aging (Azpurua and Eaton, 2015; VanGuilder et al., 2010; Vegh et al., 2014; Caterino, 2024; Stauch et al., 2014; Graham et al., 2021). Interestingly, PKR and phosphorylation of eIF2α levels in the brain decline with aging and age-related neurodegenerative diseases, and their downstream effects are also age-related (Hussain and Ramaiah, 2007). However, the relationship between age-related changes in synaptic proteins and the ISR, as a regulatory mechanism of the proteome, remains unexplored at the local level of synapses.

Here, we aimed to investigate the presence, activity, and spatial

configuration of the activated PKR-eIF2α axis in synapses and to define the contribution of PKR in maintaining synaptic proteostasis over time. We found that the PKR-eIF2α axis is present and active at synapses and that PKR regulates synaptic composition, layout, and protein synthesis, supporting a new role for PKR as a regulator of structural plasticity.

2. Material and methods

2.1. Reagent specifications are listed in the Supplementary Material

Animals. Wild-type (WT) C57BL/6 adult male mice were obtained from Jackson Laboratories (Bar Harbor, ME, USA). PKRKO mice, which have a C57BL/6 background, were generously provided by our collaborator, Dr. Mauro Costa-Mattioli. Both WT and PKRKO young (2-3 m.o.) and aged (9–12 m.o.) mice were housed in groups of four to five per cage in a humidity-controlled environment at 21 °C, under a 12-h light/dark cycle, with *ad libitum* access to food and water. All animal care and experimental procedures followed the guidelines outlined in the *Guide for the Care and Use of Laboratory Animals* (Commission on Life Sciences, National Research Council, National Academy Press, 1996) and complied with the regulations set by the National Fund for Scientific and Technological Research (FONDECYT-Chile).

Primary cell culture of hippocampal neurons and glial cells. Low-density primary hippocampal neuron cultures were prepared following a modified version of the protocol described by Kaech & Banker (Kaech and Banker, 2006). Briefly, hippocampal neurons were cultured on poly-l-lysine-coated coverslips, suspended above a glial feeder layer, in supplemented Neurobasal Medium. Glial cultures were obtained from the brain hemispheres of 1- to 2-day-old C57BL/6 pups. Meninges were carefully removed under a microscope using ultra-thin forceps. The cleaned brain tissue was then chopped in Hank's Balanced Salt Solution (HBSS) and incubated in 2.5 % trypsin supplemented with 1 % DNase for 15 min at 37 °C. Tissue disaggregation was performed by sequentially passing the sample through serological pipettes of decreasing diameters (20 mL, 10 mL, and 5 mL, 15 times each). The resulting suspension was filtered through a cell sieve to remove aggregates and centrifuged at 1000 rpm for 10 min at room temperature. The obtained pellet was resuspended in glial medium, consisting of Minimal Essential Medium (MEM) supplemented with 0.6 % (wt/vol) glucose, 100 U/mL penicillin, 100 μg/mL streptomycin, and 10 % (vol/vol) horse serum. The resuspended glial cells were cultured in T75 flasks, with the medium replaced the following day and subsequently changed every 2–3 days. Once the glial culture reached 70 % confluence, cells were detached using trypsin/EDTA, resuspended in a fresh glial medium, and seeded onto poly-l-lysine-coated 12 mm coverslips placed in 12-well plates. These glial feeder layers were cultured for 14 days before the introduction of hippocampal neurons, under 5 % CO_2 at 37 °C in Neurobasal Medium supplemented with GlutaMAX-I and B27, without antibiotics. Hippocampal neurons were obtained from embryonic mice at gestational days 16–18. Excised hippocampi were immediately transferred to HBSS in a conical tube and digested with 2.5 % trypsin. Subsequently, the tissue was gently disaggregated in neuronal adhesion medium (MEM supplemented with 0.6 % (wt/vol) glucose and 10 % (vol/vol) horse serum). Disaggregation was performed by passing the tissue through flame-polished Pasteur pipettes with blunt edges. Hippocampal neurons (30,000 cells/well) were seeded onto 18 mm coverslips, which were elevated by wax dots to create separation from the well bottom. Cells were incubated in a neuronal adhesion medium for 3 h and transferred to a 12-well plate containing the pre-established glial culture. One-third of the culture medium was replaced every 7 days with fresh Neurobasal Medium until the experimental endpoint.

Immunofluorescence. Immunofluorescence in primary cultured hippocampal neurons was performed as previously described (Farías et al., 2009). In brief, hippocampal neurons were fixed with 4 % paraformaldehyde (PFA) and 4 % sucrose in PBS containing Ca^{2+}/Mg^{2+} for 20 min at room temperature. The samples were then rinsed three times with washing solution (1× PBS with Ca^{2+}/Mg^{2+}), allowing 10 min for each wash. Next, the samples were permeabilized with 0.2 % Triton X-100 in 1× PBS with Ca^{2+}/Mg^{2+} for 20 min, followed by three additional rinses. After permeabilization, the samples were incubated in a blocking solution (0.02 % gelatin in 1× PBS with Ca^{2+}/Mg^{2+}) for 1 h at 37 °C. The primary antibody incubation was performed overnight at 4 °C. The next day, the samples were rinsed three times with a washing solution (10 min each), incubated with secondary antibodies, washed three more times with the same washing solution (10 min each), and then rinsed 10 times in bi-distilled water using forceps. Finally, coverslips (1.0–1.2 mm thickness) containing the samples were mounted on glass slides using Dako mounting medium. The samples were stored at room temperature and protected from light. Negative controls of immunofluorescence and antibody specifications are shown in the Supplementary Material File.

***In vitro* transfection of cultured hippocampal neurons.** Transfection was performed using a plasmid containing Enhanced Green Fluorescent Protein (EGFP) obtained from Clontech (Mountain View, CA). Neurons were cultured as previously described and transfected with the EGFP plasmid on day 3 of culture. Transfection was performed utilizing Lipofectamine 2000 as a vector in OptiMEM medium. The transfection mix comprised of 0,4μg of EGFP plasmid and 4 μL of Lipofectamine 2000. OptiMEM medium with only 4 μL of Lipofectamine 2000 was used as a control. After transfection, immunofluorescence against PKR or p-PKR (Thr446) was performed at 14 or 21 *in vitro* days.

Confocal image acquisition, processing for analysis, and replication strategy. For the analysis of synapse colocalization and local intensity analysis, *Z*-stacks of ten neurites from the first to the second branch of neurons in three independent cultures at immunofluorescences described before were imaged using an OLYMPUS FV1200 confocal microscope with a 60× oil immersion objective (1.43 Numerical aperture) using immersive oil (refraction index 1.518) at high definition (2048 × 2048 pixels). All samples were placed on coverslips with a thickness of 0,17 μm. *Z*-stacks were acquired with 160 nm step intervals along the *Z*-axis between each focal plane, using the 2.5× zoom function in the confocal microscopy software (OLYMPUS FV10-ASW ver.04.02). Following image acquisition, maximum intensity projections were generated for each Z-stack using ImageJ software. These projections produced a single-plane image from each Z-stack, which was then used for further image processing and analysis. All experiments involving primary neuronal cultures were conducted using three independently prepared culture batches, which served as biological replicates ($n = 3$). For each biological replicate, technical duplicates were included to assess intra-experimental reproducibility. Quantitative analyses (*e.g.*, neurite or synaptic puncta measurements) were performed on data pooled from these three independent cultures, each including two technical replicates. Thus, the total number of analyzed synapses or neurites reflects biologically independent experiments, not multiple imaging fields from a single culture. Images used for quantification were randomly selected from each replicate. Quantitative measurements, including puncta size and fluorescence intensity, were conducted under masked conditions to minimize experimental bias. The number of independent replicates and the quantification strategy for each figure are explicitly described in the corresponding figure legends.

Qualitative analysis of PKR/eIF2α axis distribution in hippocampal neurons. To determine the intensity distribution of the ISR proteins, PKR, and eIF2α, we utilized a cleaned maximum projected image of the neuron. To clean the image, we created a mask using manual thresholding and then applied this mask to eliminate background noise from the original image using the clear outside algorithm. This process generates a clean image, which can be projected onto a 3D model using the ImageJ software's 3D Surface Plot feature, specifically in the ISR channel. The settings used were (Mode: filled; Grid size: 512; FireLUT, Smoothing 0; Perspective: 0; Lighting: 0,3; Scale: 1,22; *Z*-scale: 0,1; Min: 6 %; Max: 100 %).

Qualitative analysis of the presence of ISR components in 3D reconstructed dendritic spines. The images of neurons transfected

with EGFP and stained with PKR or p-PKR (Thr446) were used for 3D reconstruction. Confocal microscopy imaging was performed by Z-stacking at Nyquist resolution with a 60× oil immersion objective. These conditions enabled the resolution of structures within the specified size range for *in vitro* dendritic spines (nanometers). 3D morphometry and qualitative analysis of ISR molecular components in neuronal structures were performed in deconvolved 3D reconstructions of EGFP-transfected neuronal processes captured through confocal microscopy. Aberrations induced by the setup were corrected by determining the mean empirical Point Spread Function (PSF) by applying the same protocol to perfectly spherical beads. Deconvolution was performed on Professional Huygens software (version 16.1). To deconvolve, images were converted to 12-bit tiff format and split per fluorescence channel. Channel 1 contains the EGFP-stained cytoplasm, and channel 2 contains the PKR or p-PKR stain. Signal-to-Noise Ratio (SNR) was determined per channel, using the estimated lowest and highest values of signal intensity in the image. Then, each channel intensity was manually thresholded to isolate the signal from the background and subsequently deconvolve only the signal. Thresholded images were deconvolved with Huygens Professional 3.0.0p5 (Scientific Volume Imaging B.V.). The deconvolution parameters used were the same as the confocal setting acquisition for each channel. (Numerical aperture = 1.4, the oil index = 1518, mounting medium index = 1.372, Confocal aperture = 105 μm).

Colocalization analysis. To assess colocalization, we established two conditions: 1) a positive intensity must be present, and 2) a spatial correlation between the two signals studied (Li et al., 2004a; Bolte and Cordelières, 2006). Colocalization was analyzed between the signal of an ISR protein and either a presynaptic or postsynaptic marker. To achieve this, we examined the correlation of the signal intensities using the intensity correlation analysis (ICA) described in (Li et al., 2004a) and the spatial correlation with Van Steensel's analysis described in (Bolte and Cordelières, 2006). All analyses were performed using Fiji (Schindelin et al., 2012), including ImageJ software 1.54p (Schneider et al., 2012). The colocalization analysis of dendritic spines was performed on images of the second and third-order dendritic branches of hippocampal neurons with pyramidal-like morphology (Banker and Cowan, 1979; Benson et al., 1994). Intensity correlation measurements were performed on immunofluorescence image pairs of different dendritic spines. The ICA analysis produces an intensity correlation quotient (ICQ) representing the relationship between the analyzed signals. The ICQ values obtained from the ICA analysis range from −0.5 to +0.5. When the ICQ is approximately 0, it indicates random staining; when the ICQ varies between the range of $0 > ICQ > -0.5$, it represents segregated staining, and dependent staining when ICQ values vary $0 < ICQ < +0.5$. A perfect colocalization is interpreted when ICQ = 0.5 (Li et al., 2004a). Spatial correlation or random distribution of partially co-localized images was determined using Van Steensel's cross-correlation analysis with the JACoP plugin of ImageJ software, applying 20 nm lateral displacements to the immunofluorescence image pairs (Bolte and Cordelières, 2006). Both the ICA and Van Steensel's analyses were performed using a custom semi-automatic quantification and segmentation program on Fiji software. The segmentation and intensity correlation analysis (SICA) program generates a mask around the neurite using threshold segmentation on the channel that resembles the neurite's structure. (This channel is selected through careful observation of the images). The perimeter of the mask is superposed on the different channels, while the outer background of the perimeter is erased, thus eliminating false zero correlation values in all channels. For the analysis of intensity variation between conditions, we employed two methods. The first method was global intensity analysis, used to quantify intensity across the entire area of the selected neurite after segmentation, which we referred to as neurite intensity. The second method was the local intensity analysis, which was performed exclusively on the synaptic positive perimeters according to the pre or postsynaptic marker used. Both the global and local analyses were performed simultaneously using a custom quantification and segmentation program in Fiji software. For the global intensity analysis, we used the same neurite segmentation method described earlier. For the local intensity analysis, we modified the following steps: once the neurite segmentation was completed, we used the Bernsen (Radius = 3) local binarization method (Bernsen, 1986) on the pre or postsynaptic channel to generate a second mask that included only the perimeter of the positive areas of the synaptic markers. Finally, we used size exclusion by removing the selected areas whose sizes do not correspond to a synaptic mark and the size corresponding to background noise. This was accomplished using a lower and upper size threshold. Afterward, the cleaned synaptic positive perimeter was superposed on the channel of interest, and the rest of the image was erased. This program, here referred as SALIA, which stands for Segmentation and Local Intensity Analysis. Using the SALIA methodology, we can analyze only the positive synaptic areas of the channel of interest, thus allowing us to measure the local intensity in those areas. Macros Scripts are available in the Supplementary Material Files.

Poly I:C Transfection in Conditioned Mouse Hippocampal Neuronal Cultures. To study eIF2α activation *via* PKR kinase, Poly I:C (5 μg/μL) was used as an activating stimulus as previously described (Scarim et al., 2001) in conditioned neuronal cultures of 14DIV mouse hippocampal neurons. Fresh working solutions were prepared under a laminar flow hood. For PKR activation in hippocampal neurons, Poly I:C was transfected using Lipofectamine 2000. For this, the transfection solution was prepared by dropwise adding 20 μL of Lipofectamine 2000 to 6.5 mL of Poly I:C diluted in OptiMEM. As control, Lipofectamine 2000 diluted in OptiMEM medium was used. These solutions were prepared and incubated for 25 min before use. To perform the transfection, the coverslips with hippocampal neurons were transferred under sterile conditions from the original plate to the transfection plate, placing the back side of the coverslip in contact with the plate, while the front side (containing the hippocampal neurons and wax spots) faced upward. Then, 500 μL of Poly I:C-containing transfection and control solution was added to the neurons, and the cultures were incubated for 30 min at 37 °C and 5 % CO_2. Once the transfection was completed, the coverslips were transferred back to their original plates, under sterile conditions. After 3 h at 37 °C and 5 % CO_2, cells were processed for immunofluorescence.

Synaptic layout analysis. Pre and postsynaptic areas were segmented as mentioned in the 'Qualitative analysis of the presence of ISR components in 3D reconstructed dendritic spines' section. Following segmentation, binarization was performed. Then, binary particles were filtered at the lower tail of their size distribution, considering the resolution of our optical system for each specific channel (wavelength) and at the higher tail, considering previously reported sizes of synapses from references (Maiellano et al., 2023; Roque et al., 2014; Schikorski and Stevens, 1997). After filtering, pre or postsynaptic particles numeric densities, integrated densities (intensity per area) and sizes were determined using the particle analyzer in Image J software.

Synaptoneurosomes extraction. Synaptoneurosomes (SN) preparations contain isolated pre and postsynaptic components surrounded by a double-layer membrane (Michaelis et al., 2017; Davis and Bloom, 1973). SNs were obtained through subcellular fractionation. SNs were prepared from frozen brain tissue. For this, we extracted the cortex or hippocampus from adult WT (C57BL/6) or PKRKO mice of different ages. To this end, mice were euthanized using CO_2 intoxication in concordance with the bioethics committee immediately before tissue extraction. Then, we separated the mouse head using a surgical scissor. Immediately, the brains were exposed by removal of the cranial vault, making a complete bilateral section of the crania from the foramen magnum to the anterior nasal aperture. Afterward, the brains were extracted, pushing gently with ultra-thin forceps. Then, the isolated brains were submerged in cold PBS1X (4 °C). Under those conditions, brain hemispheres were separated, and a sagittal cut was made between both hemispheres using a razor blade. Then, cortices and hippocampi were isolated from each hemisphere using ultra-thin forceps (Dummont N°5). Finally, cortices and hippocampi were collected in dry ice and then

stored at −80 °C for at least a week. Once the frozen period was over, we performed the SNs extraction using Syn-PER buffer supplemented with proteinases and phosphatases inhibitors of the following mix: phenylmethylsulfonyl fluoride 1 mM, sodium fluoride 5 mM, leupeptin 0.01 mM, sodium orthovanadate 1 mM, pepstatin A 1 μM, glycerol phosphate 1 mM, antipain 1 μM. For SNs preparation, 1 mL of Syn-PER reagent was added to 0.1 g of tissue, and the tissue was disaggregated in a glass douncer using up-and-down homogenization twenty times, followed by twenty repetitions of homogenization with a tighter douncer. Then, samples were transferred to a 1.5 mL Eppendorf tubes and centrifuged at 1200 *g* for 10 min at 4 °C to eliminate the tissue debris. An aliquot of the supernatant (containing the homogenate (H) fraction) was stored at −80 °C for subsequent analysis. The supernatant was centrifuged at 15000 *g* for 20 min at 4 °C to obtain the cytosolic (C) and synaptoneurosomal (S) (pellet) fractions that were stored at −80 °C for analysis.

Puromycin incorporation determination in synaptoneurosomes. First, a pellet containing the synaptoneurosomal fraction from a whole mouse brain was prepared as described above and maintained at 4 °C. Four WT and four PKRKO animals were used, with each animal considered as a single *n*. Each synaptoneurosomal pellet was resuspended in Translation Buffer (TB: 11 mM NaCl, 4.7 mM KCl, 1.2 mM $MgSO_4$, 2.5 mM $CaCl_2$, 1.53 mM KH_2PO_4, 212.7 mM glucose, and 1 mM dithiothreitol) at 4 °C. The synaptoneurosomes were then washed twice by centrifugation at 10,000 rpm for 10 min at 4 °C, by resuspension in cold TB after each spin. A third centrifugation was performed under the same conditions, but the synaptoneurosomes were resuspended in TB at 37 °C and incubated for 5 min. Each sample was then divided into equal volumes to generate the experimental conditions: Control (TB), puromycin incorporation (PURO), and puromycin incorporation under protein synthesis inhibition (PURO + CHX). Puromycin incorporation was achieved by adding 50 μg/mL puromycin to the synaptoneurosomes and incubating at 37 °C for 15 min. Protein synthesis inhibition was performed in parallel by co-treating with 200 μg/mL cycloheximide during puromycin incubation at 37 °C for 15 min. After incubation, samples were returned to 4 °C and washed three times by centrifugation and resuspension in cold TB as described above. Finally, the samples were processed for western blotting.

Electron microscopy. Material from the synaptic fraction was fixed overnight by immersion in 2.5 % glutaraldehyde, 0.01 % picric acid, 0.1 M cacodylate buffer, pH 7.4. Then, synaptoneurosomes samples were rinsed in the same buffer and immersed in 1 % OsO4 for 1 h, followed by incubation with 2 % uranyl acetate for 2 h. Synaptoneurosomes samples were dehydrated with a graded ethanol and propylene oxide series and infiltrated with Epon from Ted Pella Inc. Ultrathin sections were contrasted with 1 % uranyl acetate and lead citrate. Grids were examined with a Phillips Tecnai 12 electron microscope operated at 80 kV. Negative films were developed and scanned.

Immunoblot Analysis. Proteins were run in a 10 % SDS-polyacrylamide gel and transferred to a PVDF membrane using a wet Trans-Blot Turbo System from Bio Rad. To evaluate samples from synaptoneurosomal extraction, 30 μg of total protein from each fraction was loaded on the gel. The PVDF membrane was incubated with a blocking solution (TBS 0.1 % Tween-20, 10 % BSA) for 1,5 h. First, antibodies were diluted in a TBS 0.1 % Tween-20, 3 % BSA solution and incubated overnight at 4 °C. After three 10-min washes, the membrane was incubated with secondary antibodies in a TBS 0.1 % Tween-20 solution for 1.5 h at room temperature. After three washes with a 0.1 % Tween-20, 3 % BSA solution in TBS, the membrane was rinsed three more times with TBS 0.1 % Tween-20. Finally, the membrane was analyzed using the equipment ChemiDoc. Full membranes and antibodies specifications are shown in the Supplementary Material Files.

Statistical Analysis. Statistical analyses were performed using GraphPad Prism (San Diego, CA, USA, version 10.5.0). Data are expressed as mean ± S.D. For protein levels comparisons by Western blot, we used experimental groups with $n = 3$, 4, or 6 (see Figure Legends). Each experimental unit (*n*) corresponded to a distinct animal. Immunofluorescence image analyses (including intensity correlation, mean intensity, normalized integrated density, and pre/post-synaptic puncta measurements) were performed using experimental groups with $n = 30$. Specifically, three independent neuronal cultures were prepared from a single litter of mice. For each experiment, all conditions were performed using two replicate wells. Ten neurites were analyzed per well pair per culture, resulting in a total of 30 neurites (10 per group/condition). The Shapiro-Wilk test was used to assess whether data followed a normal (Gaussian) distribution, with a significance level (α) of 0.05. Data with normal distribution was analyzed using a Welch's *t*-test (confidence interval = 95 %; significance threshold: $p \leq 0.05$). Effect size was calculated using Cohen's $d = (\bar{x}_1 - \bar{x}_2)/s_p$., where $\bar{x}_1$ = mean of group 1, $\bar{x}_2$ = mean of group 2 and s_p = pooled standard deviation. When this difference is not significant, the effect is not mentioned. Data not normally distributed was analyzed using a one-tailed Mann–Whitney test (confidence interval = 95 %; $p \leq 0.05$). Figs. 7, 8, and 9 were analyzed using Two-tailed Mann–Whitney tests, except Fig. 8A, where a Welch's t-test was applied. One-tailed Mann–Whitney tests were employed in specific cases (Fig. 1, Fig. 2, and Fig. 3) where prior evidence supported a directional hypothesis. For Synapsin and PSD95 enrichment analyses in synaptosomal fractions, a previous directional hypothesis exists regarding their enrichment. For the PKR and phospho-PKR enrichment analyses (Fig. 1A) our biochemical fractionation demonstrated almost exclusive presence of these proteins in the synaptic fraction, with no detectable levels in the cytosolic fraction. Therefore, the statistical comparison was confirmatory rather than exploratory, justifying a directional (one-tailed) analysis. For eIF2α and phospho-eIF2α, two-tailed tests were employed. In analyses comparing synaptic protein levels between young and aged animals, previous studies have reported age-associated decreases in Synapsin (VanGuilder et al., 2010; VanGuilder et al., 2011), PSD95 (VanGuilder et al., 2010), and eIF2α levels (Hussain and Ramaiah, 2007; Ladiges et al., 2000) and provide the rationale behind this choice, along with data from our lab. Based on these reports, we hypothesized a directional reduction with aging and accordingly used one-tailed tests. A *p*-value of <0.05 was considered statistically significant.

3. Results

PKR, p-PKR, eIF2α, and p-eIF2α are present at CNS synapses, where their levels and activation are modified with aging. The PKR branch of the ISR in the brain acts as a memory repressor, and its genetic or pharmacological downregulation has been shown to promote long-lasting changes in synaptic function and to enhance different types of long-term memory (Costa-Mattioli et al., 2005; Costa-Mattioli et al., 2007; Hwang et al., 2017; Placzek et al., 2016; Zhu et al., 2011; Stern et al., 2013). In addition, local translation has been reported to be important for long-lasting changes in synaptic function (Nguyen et al., 1994; Kang and Schuman, 1996). Given this, it is possible that the PKR-branch of the ISR exerts its role locally at synapses. However, the specific localization or distribution of PKR and eIF2α at synapses remains largely unknown. To address this issue, we investigated the localization of PKR, eIF2α, and their phosphorylated forms at hippocampal synapses *in vivo*. Briefly, we isolated fractions enriched in both pre and post-synaptic components, referred to as synaptoneurosomes, from hippocampal homogenates of WT mice. Ultrastructural analysis by electron microscopy (EM) consistently revealed the expected pre and post-synaptic structures in the synaptoneurosomal fractions (Fig. S1). Moreover, we observed the expected enrichment of Synapsin (SYN) and PSD95 (pre and postsynaptic markers, respectively) in the synaptic fractions obtained from the hippocampus (Fig. 1A) and the cortex (Fig. S3A). We then analyzed the distribution of PKR and eIF2α, along with their phosphorylated forms, in the synaptic and cytosolic fractions, assessing their activation status by measuring the ratio of phosphorylated PKR to total PKR (p-PKR/PKR) or phosphorylated eIF2α to total eIF2α (p-eIF2α/eIF2α) (Fig. S2A and S3A). Our results show that PKR

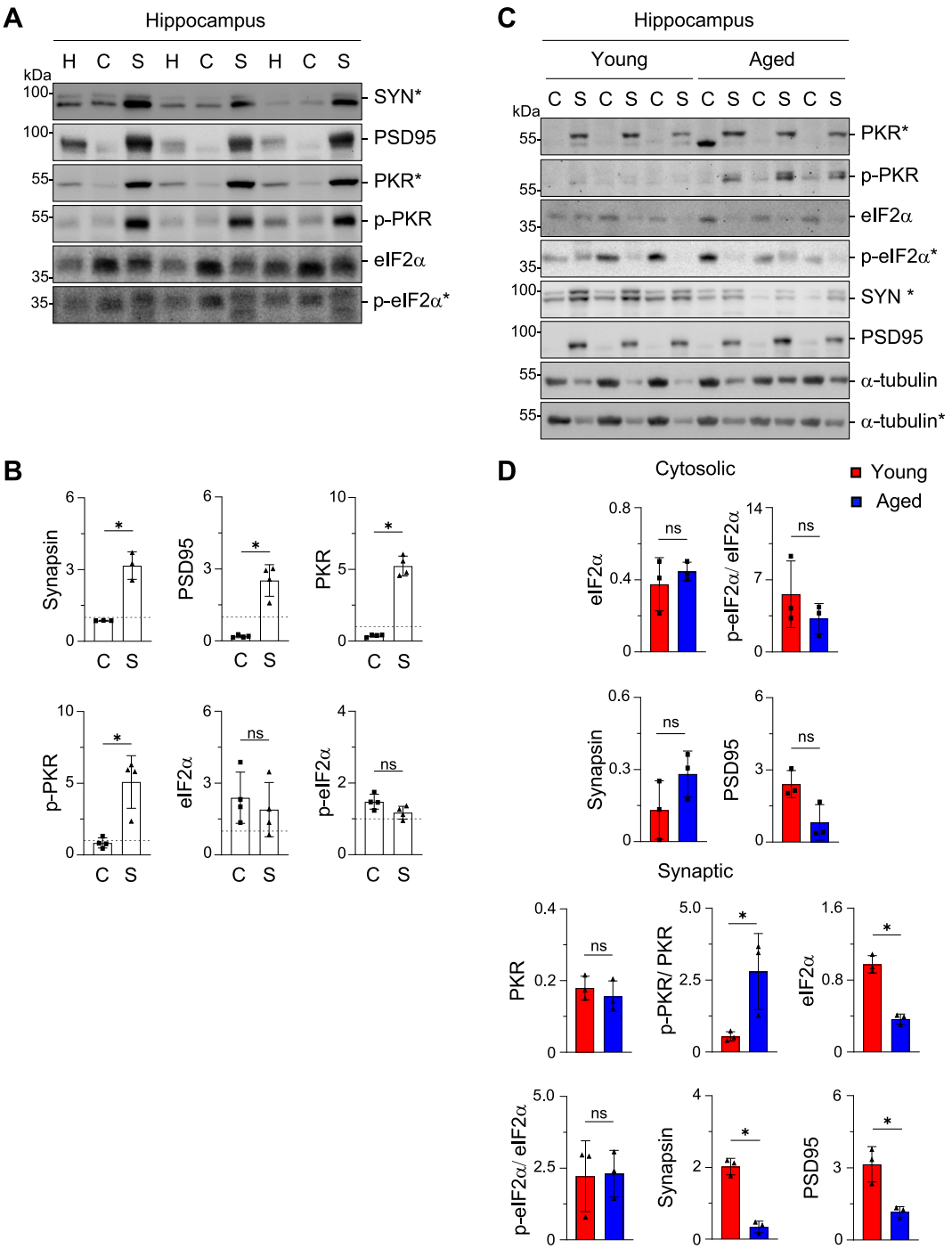

Fig. 1. PKR, p-PKR, eIF2α, and p-eIF2α are present at CNS synapses where levels and activation are modified in aging. The hippocampus from WT mice was processed into total homogenates (H), cytosolic (C), and synaptoneurosomal (S) fractions. **(A)** Synapsin (SYN) and PSD95 were used as pre and postsynaptic markers, respectively, and ISR proteins (PKR, p-PKR, eIF2α, and p-eIF2α) were detected by Western blot in H, C, and S fractions (30 μg/lane). Proteins blotted on the same membrane are tagged with an asterisk (*) or untagged. **(B)** Protein levels were determined by quantifying the intensity of bands in the C (squares) and S (triangles) fractions, normalized to their levels in the total homogenate (grey dashed line). $n = 4$; Mean ± S.D. One-tailed Mann-Whitney test: ns, not significant; $^*p < 0.05$). **(C)** Presynaptic marker, postsynaptic marker, and ISR proteins were detected by Western blot in C and S fractions (30 μg/lane) from the hippocampus of young (2–3 m.o.) and aged (9–12 m.o.) WT mice. **(D)** Quantification of protein levels in the cytosolic and synaptic fractions, normalized to the intensity of α-tubulin on the same lane, is presented (Young, red; Aged, blue). The intensity of phosphorylated eIF2α was normalized against its total form. $n = 3$. For SYP, PSD95, PKR, and p-PKR, one-tailed Mann-Whitney test. For eIF2α and p-eIF2α, a two-tailed Mann-Whitney test. ns, not significant; $^*p < 0.05$. (For interpretation of the references to colour in this figure legend, the reader is referred to the web version of this article.)

and its phosphorylated form were significantly enriched in the synaptic fraction compared to the cytosolic fraction when normalized to their levels in the hippocampal homogenate (dashed line) (Fig. 1B). Notably, the synaptic enrichment of PKR and its activated form is comparable to that of pre and postsynaptic markers. In contrast, the distribution of eIF2α and its phosphorylated form (p-eIF2α) in the synaptic fraction was indistinguishable from that in the cytosolic fractions (Fig. 1B). Interestingly, the distribution pattern observed in the hippocampus for PKR

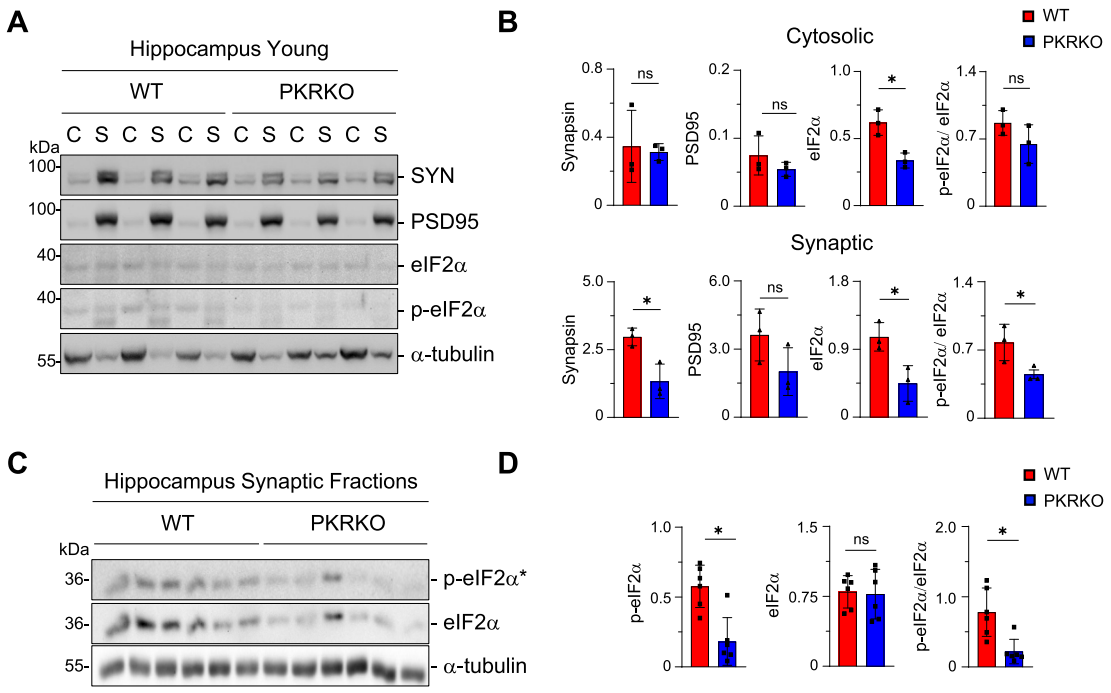

Fig. 2. PKR affects the abundances of synaptic Synapsin, eIF2α, and phosphorylated eIF2α in the hippocampus. The hippocampi from **(A)** young (2–3 m.o.) WT and deficient in the PKR-encoding gene (PKRKO) mice were processed into cytosolic (C) and synaptoneurosomal (S) fractions (30 μg/lane). Synapsin (SYN), PSD95 as pre and postsynaptic markers, respectively, eIF2α, and p-eIF2α were detected using Western blot analysis. **(B)** The levels of the proteins detected in A were determined by quantifying the band intensity of each protein in the C and S fractions, normalized to the intensity of α-tubulin on the same lane. $n = 3$; Mean ± S.D. Two-tailed Mann-Whitney test: ns, not significant; *$p < 0.05$. **(C)** The levels of eIF2α, p-eIF2α, and PSD95 were evaluated in synaptic fractions from young WT ($n = 6$) and PKRKO ($n = 6$) mice using Western blot analysis. **(D)** Quantification of the band intensity of proteins detected in the synaptic fractions in C), normalized to the intensity of α-tubulin on the same lane. Mean ± S.D. Two-tailed Mann-Whitney test: ns, not significant; *$p < 0.05$.

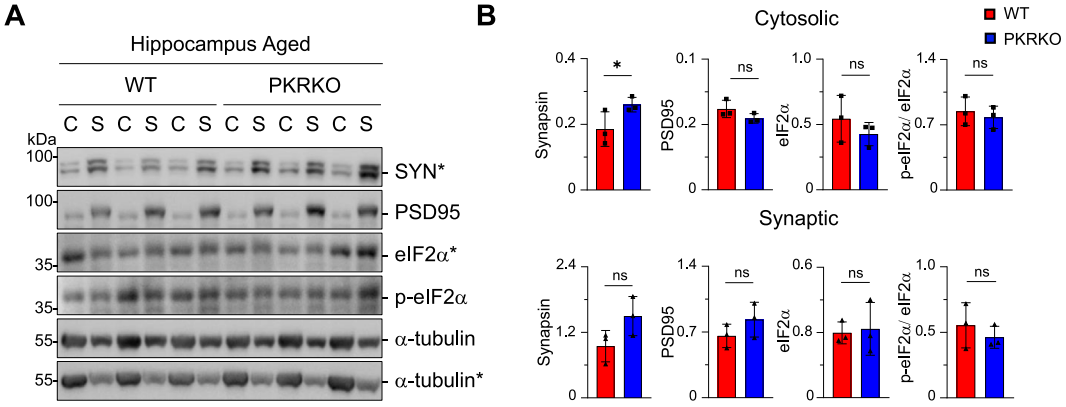

Fig. 3. The effect on synaptic Synapsin, eIF2α, and phosphorylated eIF2α abundances in the hippocampus is mitigated in aged synapses. The hippocampi from **(A)** aged (9–12 m.o.) WT and deficient in the PKR encoding gene (PKRKO) were processed into cytosolic (C) and synaptoneurosomal (S) fractions (30 μg/lane). Synapsin (SYN), PSD95 (as pre and postsynaptic markers, respectively), eIF2α, and p-eIF2α were detected using Western blot analysis. **(B)** The levels of the proteins detected in A were determined by quantifying the band intensity of each protein in the C and S fractions, normalized to the intensity of α-tubulin in the same lane. The intensity of phosphorylated eIF2α was normalized against its total form. $n = 3$; Mean ± S.D. One-tailed Mann-Whitney test: ns, not significant, *$p < 0.05$.

and its phosphorylated form is similar to the one found in the cortex (Fig. S3A). However, the distribution of eIF2α and p-eIF2α in the cortex differed from that in the hippocampus, with both proteins being enriched in the cytosolic fractions (Fig. S3A). These results indicate that while both PKR and its phosphorylated form are enriched in CNS synapses, the distribution of eIF2α and p-eIF2α varies across brain regions, with differential enrichment in synaptic and cytosolic fractions.

Inhibition of the ISR reverses age-related cognitive decline (Derisbourg et al., 2021; Derisbourg et al., 2021a; Derisbourg et al., 2021b; Krukowski et al., 2020), and the PKR branch of the ISR is activated in the aging brain and in age-related neurodegenerative diseases (Martinez et al., 2021). Thus, after confirming the presence of PKR, eIF2α, and their phosphorylated forms at CNS synapses *in vivo*, we decided to examine their synaptic levels and neuronal distribution during aging. To address this, we compared the cytosolic and synaptic distributions of PKR, eIF2α, and their phosphorylated forms in young and aged WT mice. We isolated cytosolic and synaptoneurosomal fractions from the hippocampus of young (2–3 months old) and aged (9–12 months old) WT mice and analyzed them using Western blotting (Fig. 1C). To evaluate region-specific effects and age-related changes, cortical tissue from both young and aged WT mice was processed similarly. We observed significant age-related changes in hippocampal synapses. First, the levels of PSD95 and SYN were significantly low in aged hippocampal synapses (Fig. 1D). Second, although the abundance

of synaptic PKR in synaptoneurosomal fractions did not change between young and aged mice, the phosphorylation of PKR (ratio p-PKR/PKR) was significantly increased in aged synaptic fractions (Fig. 1D). The maintenance of the synaptic distribution of PKR during aging was also observed in the cortex, but not the increase in p-PKR/PKR ratio (Fig. S3B). Third, the total levels of eIF2α in the synaptic fractions of aged mice were significantly lower than those in young mice. Interestingly, despite the increased levels of p-PKR/PKR in aged mice, the p-eIF2α/eIF2α ratio did not change with age (Fig. 1D). The synaptic eIF2α levels and phosphorylation status depend on the brain region, as we found that cortical synapses displayed different trends: eIF2α levels were increased, and the p-eIF2α/eIF2α ratio was decreased (Fig. S3B). Moreover, the age-related decrease in synaptic eIF2α was specific to the synaptic compartment, as no changes in total eIF2α levels were observed in the brain homogenates (Fig. S4). These results show that the composition of proteins at CNS synapses changes drastically during aging, including alterations in the levels of the novel synaptic proteins PKR and eIF2α. Additionally, our results revealed the activation of the PKR branch of the ISR in aging synapses.

PKR contributes to the abundances of synaptic Synapsin, eIF2α, and phosphorylated eIF2α in the hippocampus, and this contribution is mitigated in aged synapses. Then, we investigated whether PKR regulates both the abundance and phosphorylation status of eIF2α at synapses, potentially influencing the overall synaptic protein composition. To explore this, we measured the levels of Synapsin, PSD95, eIF2α, and its phosphorylated form in the cytosolic and synaptoneurosomal fractions of the hippocampus from young mice lacking PKR (PKRKO mice; Fig. 2A, B). In young animals, PKR deficiency induced significant changes at synapses. We observed a marked reduction in the levels of eIF2α, p-eIF2α/eIF2α ratio, and Synapsin (Fig. 2A). The changes due to PKR deficiency were partially replicated in the cytosolic fractions, where we only detected a decrease in eIF2α levels, highlighting the specificity of PKR's control over synaptic protein composition (Fig. 2A). Notably, the reductions in synaptic proteins caused by PKR deficiency in the hippocampus do not occur at cortical synapses (Fig. S7A). Furthermore, when analyzing total hippocampal homogenates from young WT and PKRKO mice, we observed different results compared to synapses. Specifically, SYN levels or the p-eIF2α/eIF2α ratio remained unchanged, while PSD95 levels were decreased in PKRKO mice, and eIF2α total levels were increased (Fig. S4). We further explored the observed reduction in p-eIF2α and eIF2α in synapses by comparing the levels of phosphorylated eIF2α and eIF2α in the synaptic fractions obtained from WT and PKRKO mice (Fig. 2C). We found that in conditions of genetic deletion of PKR, there were a drastic reduction in p-eIF2α (68 %) and eIF2α (72 % p-eIF2α). Of note, in these enriched synaptic fractions, we also observed the presence of two other eIF2α kinases, PERK and GCN2, and the genetic deficiency of PKR does not affect their levels (Fig. S2C, D). PERK and GCN2 do not show the preferentially enriched localization found for PKR (Fig. S2E). These results suggest that PKR regulates synaptic protein composition in a region-specific manner in the brains of young mice, and that PKR is a major contributor to eIF2α phosphorylation at synapses.

Since PKR and its target, eIF2α, are present in synaptic fractions and show alterations in their levels or activation in the aged brain, we investigated whether PKR regulates both the abundance and phosphorylation status of eIF2α at synapses and synaptic protein composition during aging. To explore this, we evaluated the levels of Synapsin, PSD95, eIF2α, and its phosphorylated form in the cytosolic and synaptoneurosomal fractions of the hippocampus from aged mice lacking PKR (PKRKO mice; Fig. 3A, B). The eIF2α, p-eIF2α, SYN, and PSD95 levels in aged hippocampal synapses were similar in WT and PKR-deficient mice (Fig. 3A, B). Of note, in cortical synapses from aged PKRKO mice, only PSD95 exhibits changes in its levels (Fig. S7B). These findings suggest that PKR regulation of eIF2α level and activity in aged mice is compartment-specific (Fig. S8). Interestingly, aged PKRKO mice exhibited decreased levels of eIF2α (Fig. S8), in contrast with what we found in PKR-deficient young mice that showed increased eIF2α levels, indicating that PKR's regulation of eIF2α levels is age-dependent. Taken together, these results support the idea that PKR modulates key synaptic proteins, such as PSD95 and Synapsin, and this regulation occurs differentially in the cortex and hippocampus. Additionally, PKR also regulates synaptic levels of its molecular target, eIF2α, and its phosphorylation status. Importantly, these regulatory effects of PKR over other protein abundances are absent in aged synapses and are tissue-specific. The consistent presence of PKR, eIF2α, and their phosphorylated forms in synaptic fractions prompted us to thoroughly analyze their distribution within intact synaptic structures.

PKR and eIF2α along with their phosphorylated forms, are located in hippocampal synapses *in vitro*. To explore in more detail the distribution and localization of PKR and eIF2α and their phosphorylated forms in neurons, we performed immunofluorescence in hippocampal neurons cultured at low densities from mouse embryos (14DIV) (Kaech and Banker, 2006). Our analysis revealed that PKR, eIF2α, and their phosphorylated forms overlapped with the cytoskeleton marker Microtubule-Associated Protein 2 (MAP2) in both the neuronal soma and branches (Fig. S8A). In these neurons, we observed a decreasing gradient of PKR and eIF2α, as well as their phosphorylated forms, from the neuronal soma to the branches (Fig. S8B). We also detected clear focal peaks of PKR and eIF2α and their phosphorylated forms, particularly in regions corresponding to synaptic structures (Fig. S8B, C). These findings suggest that while PKR and eIF2α are widely distributed across the neuronal soma and branches, they also localize to synapse-like regions, indicating a potential role in local synaptic function. To gain further insight into the presence of PKR, eIF2α, and their phosphorylated forms at specific neuronal compartments, we analyzed their location at axons, dendrites, and dendritic spines of hippocampal neurons. For these experiments, we used the presynaptic markers Bassoon (BSN) and Synaptophysin (SYP), and the postsynaptic marker PSD95. We found that PKR, p-PKR, eIF2α, and p-eIF2α were detected at remarkably close proximity of pre and postsynaptic puncta, showing clear overlapping areas between the PKR-branch of the ISR and the synaptic markers (Fig. 4A). Moreover, we found that PKR, p-PKR, eIF2α, and p-eIF2α were consistently present at the dendritic spines of hippocampal neurons as discrete puncta (Fig. 4B). In contrast to the staining pattern found for PKR (and the phosphorylated form), which is mainly detected as puncta along dendrites, eIF2α and its phosphorylated form were detected both as puncta and homogeneously distributed in these neuron projections (Fig. 4B). Those puncta were located at the neck and head of the dendritic spines (Fig. 4B). The presence of these proteins at synaptic structures by immunofluorescence is consistent with our biochemical analysis described above.

To investigate the precise colocalization of ISR proteins with synaptic markers, we performed an Intensity Correlation Analysis (ICA) (Li et al., 2004b; Dunn et al., 2011). ICA is a method used to assess the spatial correlation between two molecular signals by comparing the intensity fluctuations of each signal across space. A key measure in ICA is the Product Difference of the Mean (PDM), which is calculated by subtracting the mean intensity of each signal from individual pixel intensities and then multiplying the deviations. If the PDM is positive, both signals tend to increase or decrease together, suggesting colocalization, while negative PDM values indicate no correlation. For ICA, the fluorescence intensity of a pixel for each ISR protein was plotted against the PDM of that pixel and pre or postsynaptic markers. Examples of plotted PDMs when analyzing pixels for PKR or eIF2α and pre or postsynaptic marker intensities, in which we mainly obtained positive values (Fig. S9). Then, we calculated the Intensity Correlation Quotient (ICQ), which is derived from PDM and represents the proportion of pixels with positive PDM values relative to the total number of pixels. ICQ values range between −0.5 and + 0.5, where values close to +0.5 indicate strong colocalization. The ICA allowed us to calculate the ICQ per pair of signals (PKR: PSD95; PKR:Bassoon; eIF2α:PSD95; eIF2α:SYP and phosphorylated forms: pre or postsynaptic) on every image. To complement

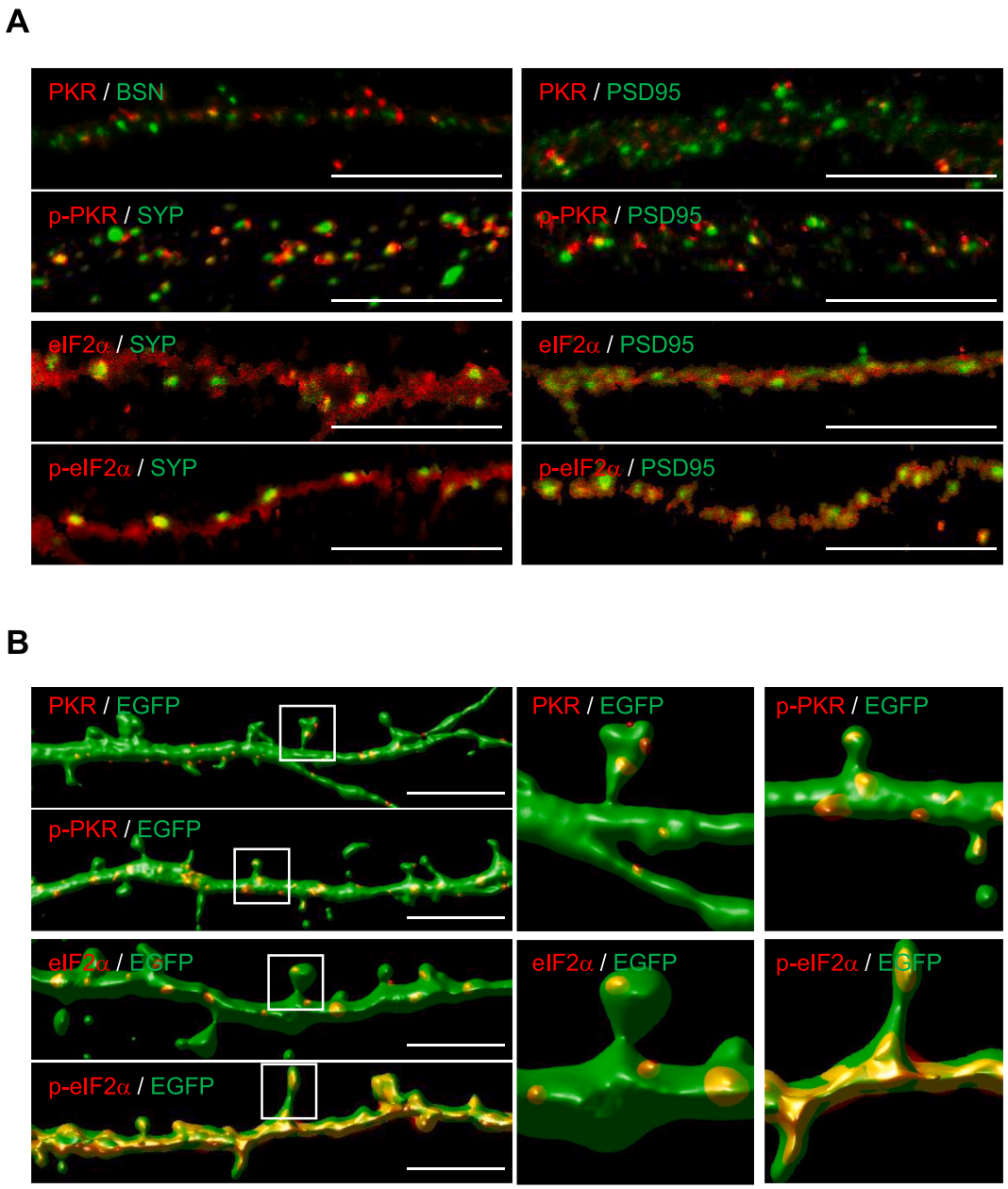

Fig. 4. PKR and eIF2α, along with their phosphorylated forms, are located in the nearby synaptic areas and in the dendritic spines of hippocampal neurons *in vitro*. Hippocampal neurons were obtained from E16 to E18 mice and cultured up to 14 days *in vitro* (14DIV) at low density to allow individual neuronal imaging. **(A)** Representative confocal images of immunofluorescence staining against PKR, p-PKR, eIF2α, or p-eIF2α (red) and pre (Bassoon/BSN) or postsynaptic (PSD95) markers (green) in the first-to-second branches of these neurons. Scale bar = 10 μm. Deconvolution and 3D reconstruction were performed on Z stacks of confocal images from the first-to-second branches of hippocampal neurons. **(B)** 3D reconstructions of dendritic spines from EGFP-transfected (300 ng/well) hippocampal neurons (14DIV) merged with the reconstructed images for PKR, p-PKR, eIF2α, or p-eIF2α staining from the immunofluorescence. An enlarged view of a specific area (white box) is shown on the right. Scale bar = 100 nm. Confocal images of immunofluorescence from entire neuronal cells can be found in Supplementary Fig. 8. (For interpretation of the references to colour in this figure legend, the reader is referred to the web version of this article.)

our analysis, we also evaluated the randomness of intensity correlation between PKR, p-PKR, eIF2α, or p-eIF2α with pre or postsynaptic markers through Van Steensel's Cross-Correlation Function (CCF) analysis (van Steensel et al., 1996) on the same images. This analysis helped us to determine whether two fluorescently labeled proteins are co-distributed in the synapse by measuring how their intensities align when one image is shifted relative to the other.

To further study the relationship between PKR, p-PKR, and synaptic markers, we applied the Intensity Correlation Analysis (ICA) method to assess the colocalization of PKR and p-PKR with presynaptic (Bassoon, BSN; Synaptophysin, SYP) and postsynaptic (PSD95) markers in immunofluorescence images of hippocampal neuron neurites (Fig. 5A, D). We generated images that depict regions where the intensity of PKR or p-PKR overlaps with the pre or postsynaptic markers, labeled as Positive Correlation (+ Corr.) along the neurites (Fig. 5A, D).

Using the PDMs distribution, we compared the intensity of PKR and p-PKR with those of pre or postsynaptic markers across the entire neurites (Fig. S9A, B). The ICA analysis revealed that most pixels were positive, indicating synchronicity in the signals between PKR and p-PKR and pre or postsynaptic markers (Fig. S9A, B; $n = 30$ per pair of stains). We quantified the mean ICQ for all pair signals, which showed positive values for each combination (Fig. 5B, E). These results provide robust

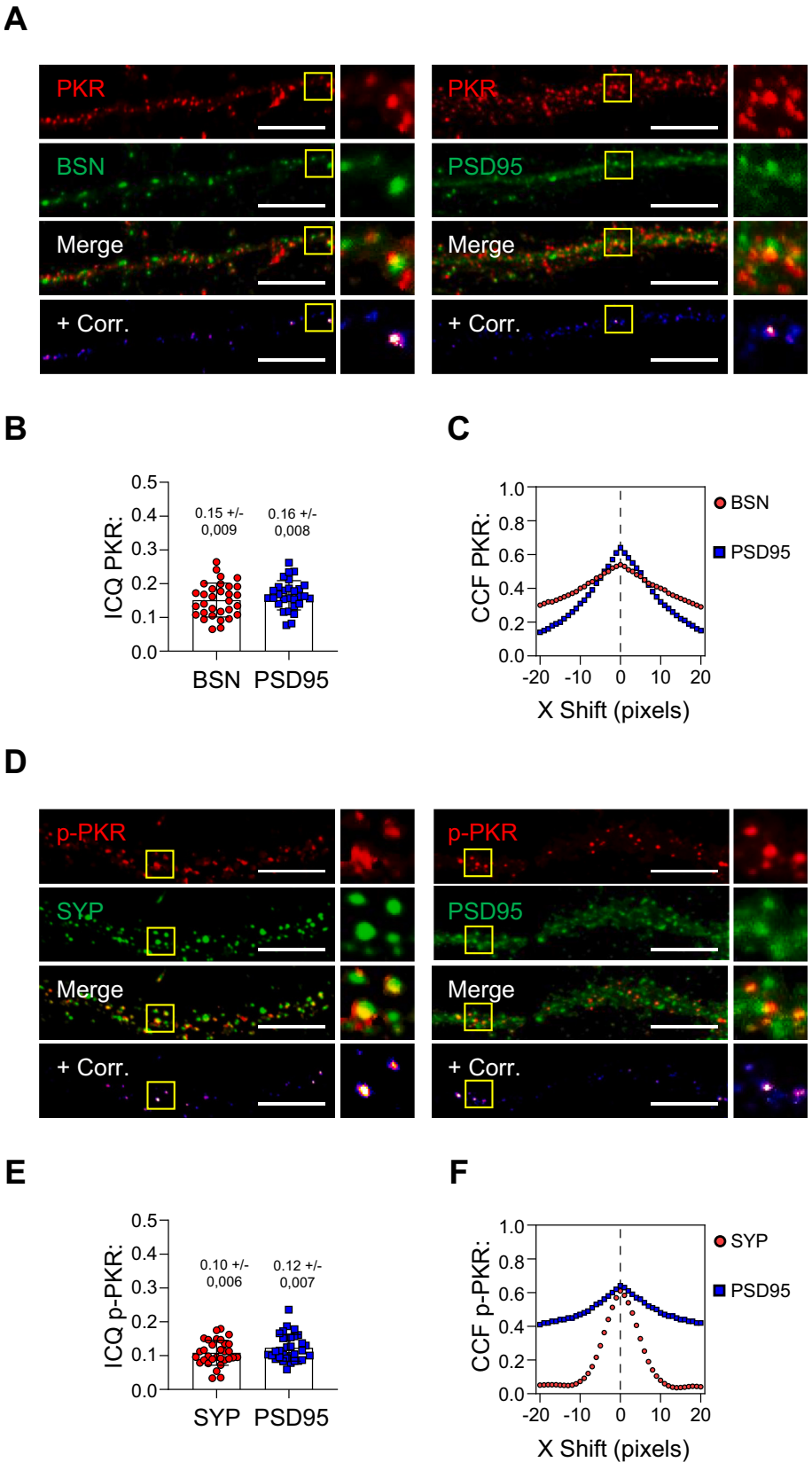

(caption on next page)

Fig. 5. PKR and p-PKR partially colocalize with presynaptic and postsynaptic markers in *in vitro* hippocampal neurons. Hippocampal neurons were obtained from E16 to E18 mice and cultured up to 14 days *in vitro* (14DIV) at low density to allow individual neuronal imaging. Colocalization and randomness of colocalization analyses were performed on Z stacks of confocal images from the first-to-second branches of hippocampal neurons ($n = 30$ per pair of markers, from images from three independent cultures). Examples of overlapping puncta (yellow square) are shown in the insets. Representative maximal projections from immunofluorescence detecting **(A)** PKR (red) and the presynaptic marker (left) Bassoon (BSN, green), and PKR (red) and the postsynaptic marker (right) PSD95 (green). Merge and positive correlation (+ Corr.) heat maps between **(A)** PKR or **(D)** p-PKR and pre or postsynaptic markers are shown. Scale bar = 10 μm. Quantification of the Mean Intensity Correlation Quotient (ICQ) between **(B)** PKR and BSN, and between PKR and PSD95, was calculated through intensity correlation analysis (ICA) at the first-to-second branches of hippocampal neurons. **(C)** Representative Cross Correlation Function (Pearson's coefficient /Δx; CCF) between PKR and BSN, and PKR and PSD95 at the first-to-second branches of hippocampal neurons. The same analysis was performed for p-PKR, detecting **(D)** p-PKR (red) and the presynaptic marker (left) Synapsin (SYN, green), and p-PKR (red) and the postsynaptic marker (right) PSD95 (green). **(E)** ICQ between p-PKR and SYN or between p-PKR and PSD95 was calculated through intensity correlation analysis at the first-to-second branches of hippocampal neurons. **(F)** CCF between p-PKR and Synapsin and p-PKR and PSD95 at the first-to-second branches of hippocampal neurons. For all panels, three independent cultures were obtained, each yielding two replicate wells. From each pair of wells, ten neurites were analyzed. Scale bar = 10 μm. For details on ICA, refer to the methodology section. (For interpretation of the references to colour in this figure legend, the reader is referred to the web version of this article.)

evidence that PKR and p-PKR signals are synchronized with the pre and postsynaptic markers, confirming their association with synaptic structures. The CCF values between PKR (Fig. 5C) and p-PKR (Fig. 5F) and pre or postsynaptic marker signals pairs decrease in response to displacement of the signals ($n = 30$ per pair of stains), revealing a nonrandom colocalization of the signals. Together, these findings demonstrate that PKR and its phosphorylated form (p-PKR) are present in synaptic regions and also colocalize with key pre and postsynaptic markers, further confirming their synaptic localization.

Next, we investigated the potential colocalization of eIF2α and p-eIF2α with pre and postsynaptic markers, using the same analysis (ICA) applied to the sensor kinase PKR. Positive regions for eIF2α and p-eIF2α were abundantly present in proximity to pre and postsynaptic puncta in immunofluorescence images at neurites of 14DIV hippocampal neurons (Fig. 6A and D, respectively). Under thorough observation, eIF2α and p-eIF2α positive regions consistently overlap with the pre and postsynaptic marker regions at all the neurites observed. Furthermore, heat maps of positive PDMs (+Corr.) of eIF2α (Fig. 6A) or p-eIF2α (Fig. 6D) at pre or postsynaptic regions indicate that variation in the intensities of ISR and synaptic signals is synchronized. Consequently, we analyzed the distribution of PDMs between eIF2α, p-eIF2α, and pre or postsynaptic signals in whole images of neurites. There, we found that a considerable part of the total pixels has intensity signals of eIF2α (Fig. S9C), p-eIF2α (Fig. S9D), and pre or postsynaptic synchronically vary. Based on this, we determined the mean ICQ between eIF2α, p-eIF2α and pre or postsynaptic markers and found that the mean ICQ was positive for all pairs analyzed (Fig. 6B, E), reflecting a positive correlation between pairs of signals. The CCF values between eIF2α (Fig. 6C) or p-eIF2α (Fig. 6F) and pre or postsynaptic markers signal pairs show a decrease in response to displacement (Fig. 6C, F), revealing a dependent variation of the signals. To our knowledge, this is the first study describing the colocalization of PKR, p-PKR, eIF2α, or p-eIF2α with pre and postsynaptic markers on neurons. When combined with our complementary biochemical evidence, these results strongly support the synaptic localization of PKR and eIF2α signaling components. This suggest that the PKR-eIF2α pathway of the integrated stress response is not only present at synapses but may also have a direct role in local synaptic regulation.

PKR activation induces local eIF2α phosphorylation at pre and postsynaptic areas. The localized presence of p-PKR and p-eIF2α at hippocampal pre and postsynaptic regions led us to test whether the phosphorylation state of eIF2α can be modulated in response to PKR activation stimulus at synapses. To explore this, we first treated neurons with Poly I:C, a commonly used dsRNA analog and a potent PKR activator (Barragan-Iglesias et al., 2020; Yang et al., 1995). After 3 h of Poly I:C transfection, we observed a marked increase in p-PKR levels in hippocampal neurons (Fig. S10). Concurrently, the levels of p-eIF2α were elevated in primary and secondary branches (Fig. 7A). Having established that PKR activation leads to increased p-eIF2α levels in neuronal branches, we next studied the phosphorylation of eIF2α, specifically at synapses under PKR activation. To achieve this, we isolated the p-eIF2α fluorescence signal and analyzed its overlap with pre and postsynaptic areas, using SYP and PSD95 as pre or postsynaptic markers, respectively. We then quantified the mean fluorescence intensity levels of p-eIF2α in both basal and PKR-activated conditions. The resulting heat maps of mean relative intensity levels of p-eIF2α demonstrated a clear increase in p-eIF2α at both pre and postsynaptic areas following Poly I:C treatment (Fig. 7B, C). These findings indicate that PKR activation leads to the localized phosphorylation of eIF2α, specifically at synaptic sites, highlighting a potential mechanism by which PKR modulates synaptic protein function through the ISR pathway.

PKR activation increases phospho-eIF2α colocalization with presynaptic regions. Building on the observation that PKR activation induces a localized increase in p-eIF2α in synaptic regions, we further investigated whether PKR activation modulates p-eIF2α localization at the pre and postsynaptic regions. Briefly, we assessed the colocalization of p-eIF2α with pre or postsynaptic markers under PKR activation conditions. We performed the ICA (Li et al., 2004b; Dunn et al., 2011) protocol on immunofluorescence confocal images from 14DIV hippocampal neurons that were stimulated with Poly I:C for 3 h after transfection. We then examined how the overlap between p-eIF2α and synaptic markers changed under control and Poly I:C conditions. Heat maps of the positive PDMs (+Corr.) at the regions where p-eIF2α and pre or postsynaptic signals overlap suggest that the intensities of these signals vary synchronously under Poly I:C treatment (Fig. 8A, B). The mean ICQ per pair of signals in every image was calculated to quantify the colocalization pattern in activation conditions compared to basal conditions. The interaction pattern for p-eIF2α:SYP changed under PKR activation conditions (p-eIF2α:SYP_{CTRL} 0.17 +/− 0,006 and p-eIF2α:$SYP_{Poly:IC}$ 0.19 +/− 0,006) (Fig. 8A). However, no changes were observed between p-eIF2α:PSD95 after eIF2α phosphorylation induction with Poly I:C (p-eIF2α:$PSD95_{CTRL}$ 0,013 +/− 0,006 and p-eIF2α:$PSD95_{Poli:IC}$ 0,0154 +/− 0,008) (Fig. 8B). The significant increase in ICQ values for p-eIF2α:SYP under Poly I:C conditions suggests an enhanced interaction or redistribution of p-eIF2α within synaptic regions marked by Synaptophysin. This shift may reflect a regulatory role of PKR activation in synaptic protein dynamics. In contrast, the colocalization of p-eIF2α with PSD95 remained unchanged after Poly I:C treatment, suggesting that eIF2α phosphorylation does not significantly impact postsynaptic density protein (PSD95) interactions. This stability implies that PKR-mediated phosphorylation of eIF2α selectively influences presynaptic rather than postsynaptic protein associations. Additionally, the CCF analysis between p-eIF2α with pre and postsynaptic markers showed no randomness in intensity correlation (van Steensel et al., 1996) on the same images (Fig. 8C), suggesting that p-eIF2α is spatially associated with specific synaptic compartments rather than being diffusely distributed throughout the cell. These results support the idea that PKR activation, through the phosphorylation of eIF2α, plays a targeted role in synaptic regulation, selectively modulating synaptic protein dynamics in response to activation conditions.

PKR contributes to the density, size, composition, and translation of synapses. The findings regarding the significant changes in structural protein constituents of CNS synapses, specifically Synapsin

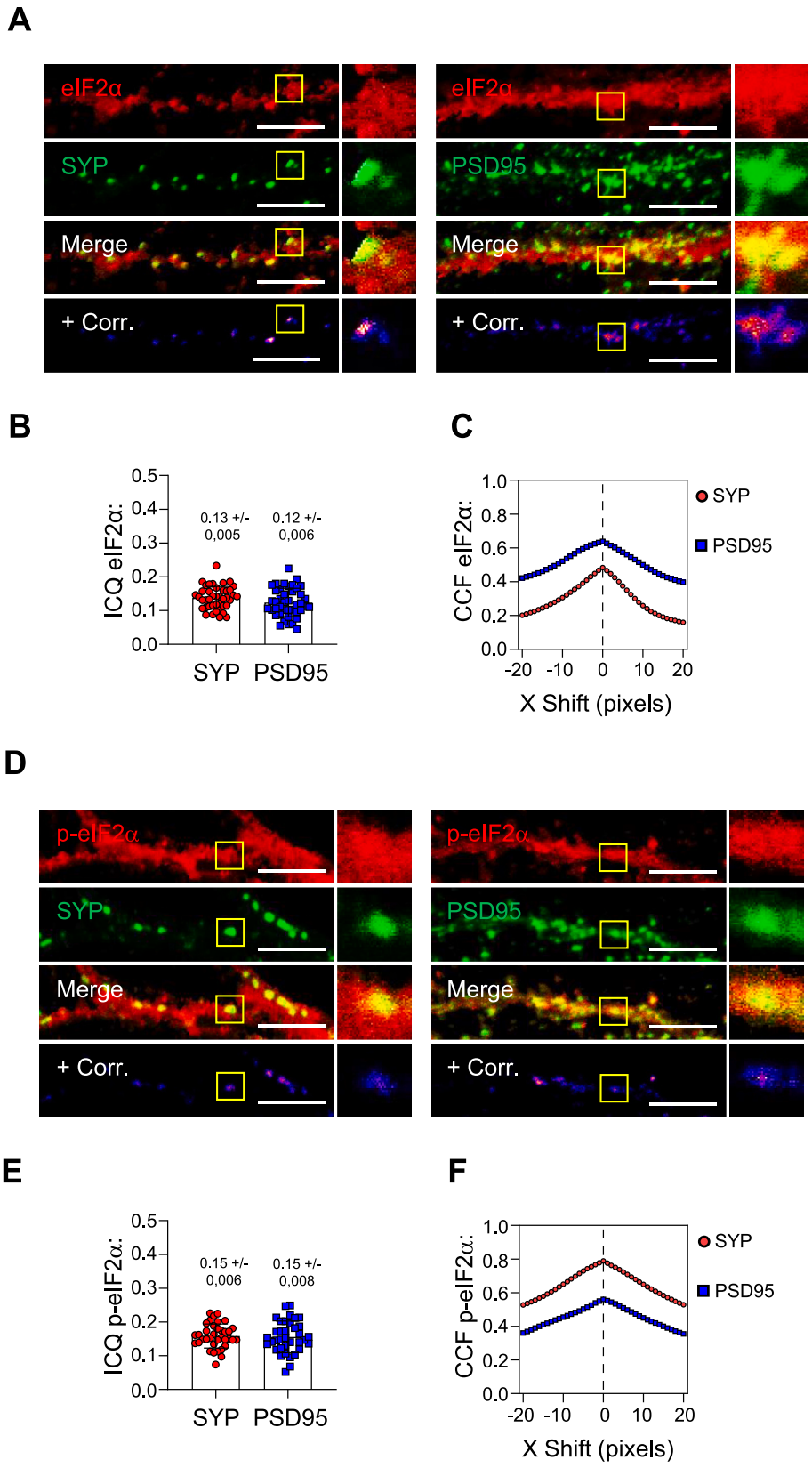

(caption on next page)

Fig. 6. eIF2α and p-eIF2α partially colocalize with pre and postsynaptic markers at hippocampal neurons *in vitro*. Hippocampal neurons were obtained from E16 to E18 mice and cultured up to 14 days *in vitro* (14DIV) at low density to allow individual neuronal imaging. Colocalization and randomness of colocalization analysis were performed on Z stacks of confocal images from first-to-second branches of hippocampal neurons ($n = 30$ per pair of markers, from images from three independent cultures). Examples of overlapping puncta (yellow square) are shown in the insets. Representative maximal projections from immunofluorescences detecting **(A)** eIF2α (red) and the presynaptic marker (left) Synapsin (SYN, green), and eIF2α (red) and the postsynaptic marker (right) PSD95 (green). Merge and positive correlation (+ Corr.) heat maps between **(A)** eIF2α or **(D)** p-eIF2α and pre or postsynaptic markers are shown. Scale bar = 10 μm. Quantification of the Mean Intensity Correlation Quotient (ICQ) between **(B)** eIF2α and BSN and between eIF2α and PSD95 calculated through the intensity correlation analysis (ICA) at the first-to-second branches of hippocampal neurons. **(C)** Representative Cross Correlation Function (Pearson's coefficient /Δx; CCF) between eIF2α and BSN and eIF2α and PSD95 at the first-to-second branches of hippocampal neurons. The same analysis was performed for p-eIF2α detecting **(D)** (left) p-eIF2α (red) and the presynaptic marker Synapsin (SYN, green), and (right) p-eIF2α (red) and the postsynaptic marker (PSD95; green). **(E)** ICQ between p-eIF2α and Synapsin (SYN) and between p-eIF2α and PSD95 was calculated through ICA at the first-to-second branches of hippocampal neurons. **(F)** CCF between p-eIF2α and Synapsin (SYN) and p-eIF2α and PSD95 at the first-to-second branches of hippocampal neurons. For all panels, three independent cultures were obtained, each yielding two replicate wells. From each pair of wells, ten neurites were analyzed. Scale bar = 10 μm. For ICA details, see methodology section. (For interpretation of the references to colour in this figure legend, the reader is referred to the web version of this article.)

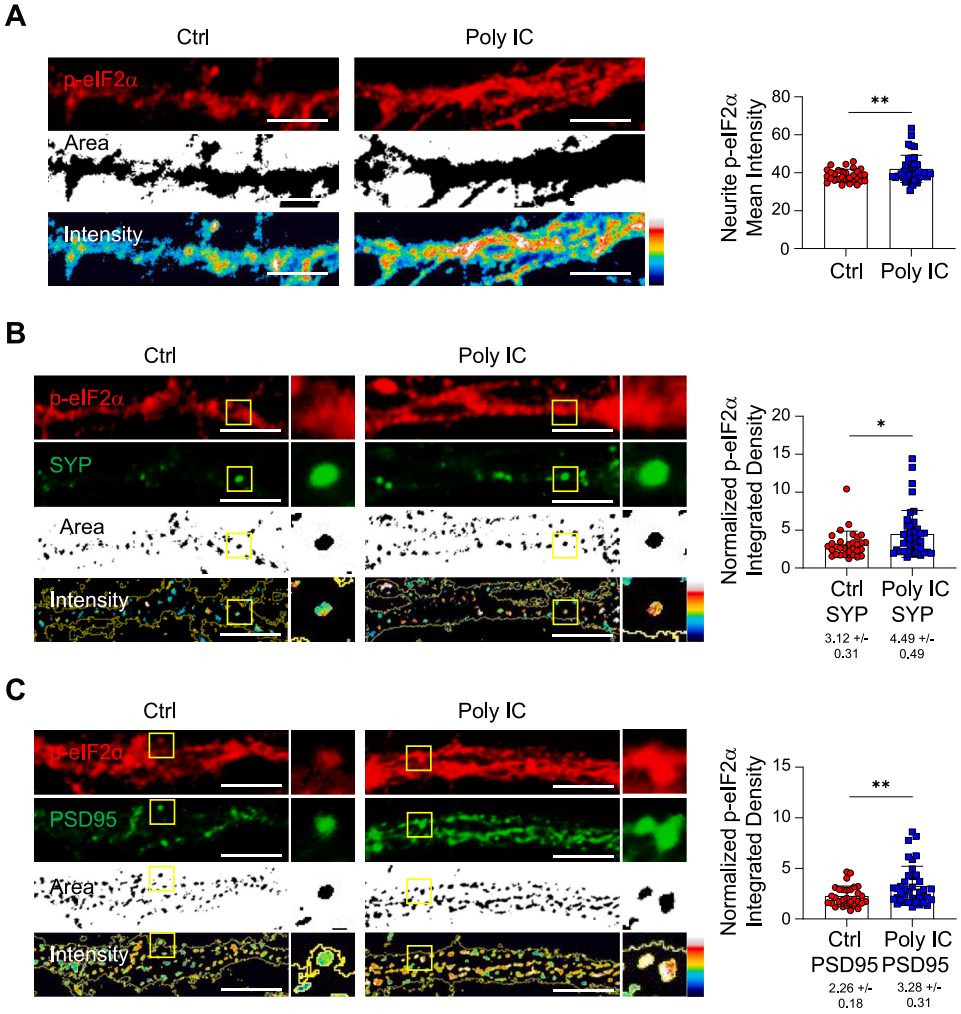

Fig. 7. Local eIF2α phosphorylation at pre and postsynaptic areas is induced by PKR activation. Hippocampal neurons were obtained from E16 to E18 mice and cultured for up to 14 days *in vitro* (14DIV). p-eIF2α intensity levels were evaluated in regions positive for pre and postsynaptic markers through immunofluorescence on those mouse embryonic hippocampal neurons at low densities to allow individual neuronal imaging. Cultures were transfected for 30 min with Poly I:C (5 μg/mL) or vehicle (Ctrl; DMSO) using Lipofectamine 2000. Then, the stimulus was removed, and after 3 h, neurons were processed for immunofluorescence. **(A)** Representative confocal images of immunofluorescence from the first-to-second branches of neurons treated with vehicle or Poly I:C (5 μg/mL) and stained against p-eIF2α (red). On the right, the quantification of mean intensity for p-eIF2α staining in neurites under vehicle or Poly I:C is shown. **(B)** Representative confocal images of immunofluorescence against p-eIF2α (red) and the presynaptic marker Synaptophysin (SYP, green) in the first-to-second branches of hippocampal neurons after 3 h of treatment with vehicle (control, Ctrl) or Poly:IC (5 μg/mL). Scale bar = 10 μm. At right, the quantification of the mean p-eIF2α integrated density at the presynaptic region, normalized to its corresponding branch integrated density, is shown for the vehicle (Ctrl; DMSO) and Poly I:C (5 μg/mL). **(C)** Representative confocal images of immunofluorescence against p-eIF2α (red) and the postsynaptic marker (PSD95, green) in the first-to-second branches of hippocampal neurons after 3 h of treatment with vehicle (Control, Ctrl) or Poly I:C (5 μg/mL). Scale bar = 10 μm. At right, the quantification of the mean p-eIF2α integrated density at the postsynaptic region normalized to its corresponding branch integrated density is shown for vehicle (Ctrl; DMSO) and Poly I:C (5 μg/mL). For all analyses, ten neurites were analyzed from images of three independent cultures ($n = 30$).; Mean ± S.D. Two-tailed Mann-Whitney test: $*p < 0.05$, $**p < 0.01$. (For interpretation of the references to colour in this figure legend, the reader is referred to the web version of this article.)

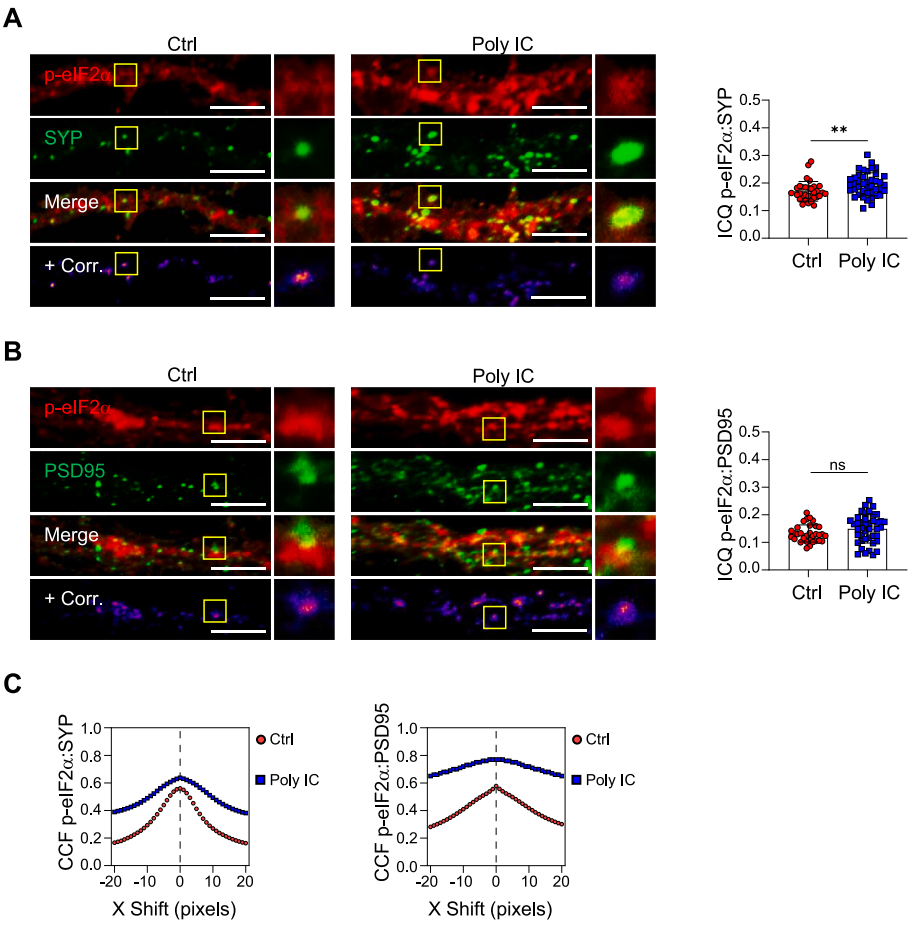

Fig. 8. Phospho-eIF2α colocalization with presynaptic areas is increased by PKR activation. Hippocampal neurons were obtained from E16 to E18 mice and cultured up to 14 days *in vitro* (14DIV) at low density to allow individual neuronal imaging. At 14DIV, cultures were transfected for 30 min with Poly I:C (5 μg/mL) or vehicle (Ctrl; DMSO) using Lipofectamine 2000. Then, the stimulus was removed, and after 3 h, neurons were processed for immunofluorescence. Colocalization and randomness of colocalization analysis were performed on Z stacks of confocal images from the first-to-second branches of hippocampal neurons ($n = 30$, per pair of markers). Examples of overlapping puncta (yellow square) are shown in insets. **(A)** Representative maximal projections from immunofluorescences detecting p-eIF2α (red) and the presynaptic marker synaptophysin (SYP, green) in hippocampal neurons treated with vehicle (Control, Ctrl) or Poly I:C (5 μg/mL for 3 h). Merge and positive colocalization (+Corr.) heat maps between p-eIF2α and SYP. Scale bar = 10 μm. Mean Intensity Correlation Quotient (ICQ) between p-eIF2α and SYP at first-to-second branches of 14DIV hippocampal neurons is shown. **(B)** Representative maximal projections from immunofluorescences against p-eIF2α (red) and the postsynaptic marker PSD95 (green) at hippocampal neurons treated with vehicle (Control, Ctrl) or Poly I:C (5 μg/mL for 3 h). Merge and positive colocalization (+Corr.) heat maps between p-eIF2α and PSD95. Scale bar = 10 μm. The mean Intensity Correlation Quotient (ICQ) between p-eIF2α and PSD95 at first-to-second branches of hippocampal neurons is shown. **(C)** Representative Cross Correlation Function (Pearson's coefficient/Δx; CCF) between p-eIF2α and SYP (left) or p-eIF2α and PSD95 (right) at first-to-second branches of hippocampal neurons treated with control (vehicle) or Poly I:C (5 μg/mL for 3 h) from images shown in A (left graph) and B (right graph). For all analyses, ten neurites were analyzed from images of three independent cultures ($n = 30$). Mean ± S.D. Two-tailed Mann-Whitney test. ns, not significant, $^{**}p < 0.01$. (For interpretation of the references to colour in this figure legend, the reader is referred to the web version of this article.)

(SYN) and PSD95, as well as alterations in eIF2α activation under PKR deficiency, prompted us to investigate the possible role of PKR in the synaptic architectural layout of newly formed synapses. For this, we studied synaptic discrete regions in conditions of PKR deficiency. To investigate this, we cultured mouse embryo hippocampal neurons at low densities from WT and PKRKO mice. These neurons developed electrically active synapses and exhibited synaptic plasticity by days 8–10 *in vitro* (Derisbourg et al., 2021b). We then conducted a detailed morphological assessment of synapses and quantitative image analysis to compare the synaptic density and size of hippocampal WT and PKRKO neurons at their primary or secondary branches at DIV14, using SYN and PSD95 stains as markers for pre and postsynaptic compartments, respectively. Our analysis revealed no significant differences in the numeric density of presynaptic (SYN puncta/μm^2) or postsynaptic (PSD95 puncta/μm^2) structures in WT and PKRKO neurons (Fig. 9A, D), suggesting that PKR is not essential for the overall number of synapses under basal conditions. However, when examining signal intensities as a proxy for protein content, PKRKO synapses displayed significantly lower SYN (Fig. 9B) and PSD95 (Fig. 9E) staining compared to WT, indicating a deficiency in the structural integrity or molecular composition of synapses. Further morphometric analysis revealed a striking alteration in presynaptic morphology: PKRKO neurons showed significantly larger mean presynaptic sizes compared to WT neurons. This increase is attributable to a reduction in medium-sized presynaptic structures (Fig. 9C), suggesting a shift in the distribution profile of presynaptic structures in the absence of PKR. In contrast, the distribution and mean size of postsynaptic compartments (PSD95 puncta) remained unaltered between genotypes (Fig. 9E, F). Given that PKR regulates the phosphorylation of eIF2α at synapses and influences the abundance of key synaptic proteins, we next sought to determine whether PKR directly modulates local protein synthesis. To address this, we isolated synaptoneurosomes from WT and PKR-deficient mice and measured *de novo* protein synthesis using a puromycin incorporation assay. Strikingly, synaptoneurosomes from PKRKO mice exhibited a significant increase in protein synthesis compared to those from WT controls (Fig. 9G). This provides direct evidence that PKR acts as a regulator of local translation

at synapses. Along with our results obtained in synaptic discrete regions, and our *in vivo* findings in synapse-enriched fractions showing altered synapse composition (decreased Synapsin levels and the proteostatic regulator eIF2α), these data demonstrated that PKR plays a critical role in modulating the molecular composition and morphological distribution of synapses, particularly within the presynaptic compartment, likely through translational control. These structural changes may underlie the previously observed synaptic functional deficits in PKR-deficient neurons, highlighting a novel role for PKR in sculpting synaptic architecture and controlling structural plasticity.

In summary, our study reveals that PKR and eIF2α, along with their phosphorylated forms, are specifically localized at central nervous system synapses. We found that aging leads to notable alterations in synaptic protein composition, characterized by increased PKR activation and a reduction in eIF2a levels at hippocampal synapses. Additionally, our data demonstrate that PKR activation plays a key role in directly modulating local eIF2α phosphorylation at synapses, highlighting the importance of the PKR-eIF2α axis in regulating synaptic function and plasticity. Importantly, we show that PKR deficiency results in a significant increase in protein synthesis in synapse-enriched fractions, providing direct evidence that PKR acts as a local regulator of translation. These findings provide new insights into how components of the ISR are integrated within synaptic compartments, suggesting a mechanistic link between ISR dysregulation, synaptic integrity, and age-related neurodegenerative processes.

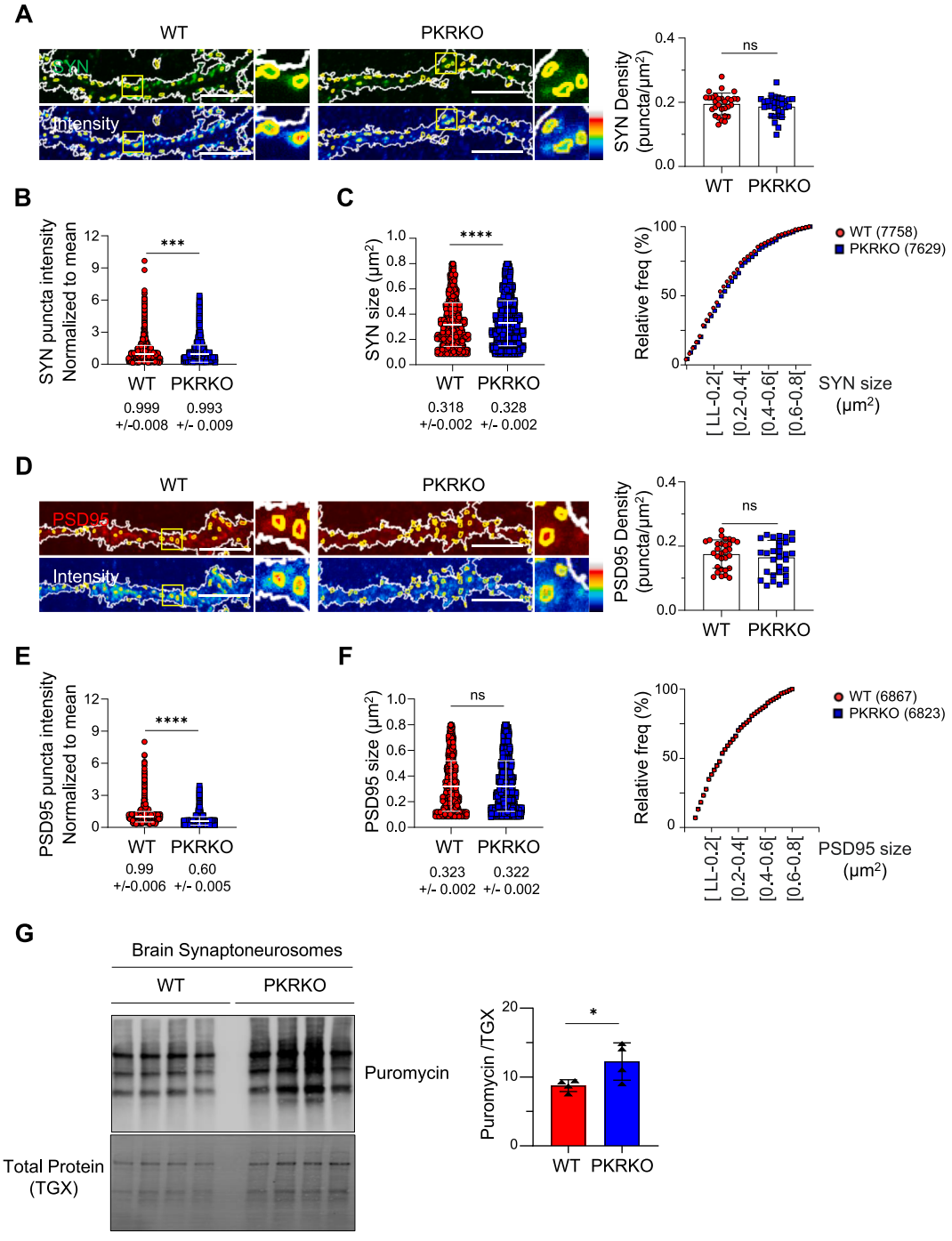

(caption on next page)

Fig. 9. PKR genetic deficiency alters synapse density, size, composition, and translation in synapses. Hippocampal neurons were obtained from E16 to E18 mice and cultured for up to 14 days *in vitro* (14DIV) at low density to allow individual neuronal imaging. Synapsin (SYN) or PSD95 positive areas were segmented from *Z*-stack maximal projections of first-to-second branches of confocal images of hippocampal neurons. After segmentation, pre or postsynaptic regions to be studied were filtered by size based on optical resolution and expected values from references (details in the Methods section). Then, SYP or PSD95 positive regions numeric densities, intensities, and sizes were determined. **(A)** Representative maximal projections from immunofluorescences against presynaptic marker SYN (green) at WT and PKRKO hippocampal neurons. Branch perimeter (white line), SYN positive regions perimeter (yellow line), and SYN positive areas intensity levels heat maps are shown. Scale bar = 10 μm. On the right, quantification of numeric densities of SYN puncta per μm^2 at branches of WT or PKRKO hippocampal neurons (n = 30; *t*-Test (Welch's); Mean ± S.D.; 95 % confidence interval. ns, not significant). **(B)** Quantification of the mean intensity of each SYN puncta normalized by the mean intensity of all puncta in the same image at branches of WT or PKRKO hippocampal neurons. **(C)** Quantification of SYN mean puncta sizes per μm^2 at branches of WT or PKRKO hippocampal neurons. On the right, the relative cumulative frequency distribution of WT and PKRKO SYP puncta sizes is shown. The number of SYN synaptic puncta quantified is indicated. LL: Lower Limit size of the first range in the distribution (see Methods). **(D)** Representative maximal projections from immunofluorescences against postsynaptic marker PSD95 (red) at WT and PKRKO hippocampal neurons. Branch perimeter (white line), PSD95 positive regions perimeter (yellow line), and PSD95 positive areas intensity levels heat maps are shown. Scale bar = 10 μm. On the right, the quantification of mean numeric densities of PSD95 puncta per μm^2 at branches of WT or PKRKO hippocampal neurons. **(E)** The quantification of the mean intensity of each PSD95 puncta normalized by the mean intensity of all puncta in the same image at branches of WT or PKRKO hippocampal neurons. **(F)** The quantification of PSD95 mean puncta sizes per μm^2 at branches of WT or PKRKO hippocampal neurons. On the right, the relative cumulative frequency distribution of WT and PKRKO PSD95 puncta sizes is shown. The number of PSD95 synaptic puncta quantified is indicated. LL: Lower Limit size of the first range in the distribution (see Methods). For all analyses, ten neurites were analyzed from images of three independent cultures ($n = 30$). Data is presented as mean ± S.D. For B, C, E, and F, a two-tailed Mann-Whitney test was applied: ns, not significant, *** $p < 0.005$, **** $p < 0.001$. **(G)** Brains from WT ($n = 4$) or PKRKO ($n = 4$) young (2 m.o.) mice were processed into synaptoneurosomal (S) fractions. S fractions were treated with puromycin (50 μg/mL) for 15 min. Incorporation of puromycin into nascent peptides was detected using an anti-puromycin antibody. The TGX signal was used as a loading control. Levels of puromycin incorporation were determined by quantifying their total lane intensity in synaptic fractions and normalized to the levels in the TGX stain on the same lane. Student's *t*-test: ns, not significant; *$p < 0.05$. (For interpretation of the references to colour in this figure legend, the reader is referred to the web version of this article.)

4. Discussion

The synapse is the fundamental unit of communication between neurons, playing a crucial role in the processing and transmission of information within the nervous system. Synaptic plasticity, the ability of synapses to strengthen or weaken over time in response to activity, constitutes the cellular foundation of learning and memory. Many morphological and functional synaptic changes observed in synaptic plasticity require *de novo* protein synthesis (Sutton and Schuman, 2006). A significant and compelling body of evidence shows that the PKR branch of the ISR is a central regulator of long-term plasticity and memory processes in both healthy and disease conditions (Costa-Mattioli et al., 2005; Costa-Mattioli et al., 2007; Zhu et al., 2011; Stern et al., 2013; Batista et al., 2016; Jiang et al., 2010; Sharma et al., 2018; Shrestha et al., 2020) (reviewed in (Costa-Mattioli et al., 2007; Lockshin and Calakos, 2024)). However, whether the ISR components are localized to the synapse and play a role in regulating the composition or morphology of synapses remains largely unknown. In this study, we used two complementary assays to investigate the presence of PKR and eIF2α, along with their phosphorylated forms, at synapses in both *in vivo* and *in vitro* models. Our findings revealed that PKR is active (phosphorylated) at synapses (Fig. 1A), and its local activation leads to the phosphorylation of eIF2α at these synapses (Fig. 7B, C). Using mice lacking PKR, we found that PKR regulates eIF2α phosphorylation (Fig. 2A, B) and Synapsin levels at synapses in young animals (Fig. 2A), and contributes to synapse size (Fig. 9, C) and protein synthesis in synapses (Fig. 9G). Interestingly, synapses from aged mice exhibited increased PKR activation and reduced eIF2α levels (Fig. 1C, D), supporting the role of these ISR components in age-dependent neurodegeneration. Overall, our results show that the PKR-eIF2α signaling axis is present at hippocampal and cortical synapses, exhibiting region-specific and age-dependent alterations. This local ISR activation changes the synaptic protein composition, size, and morphology, providing new insights into the roles of PKR and eIF2α in synaptic function.

Synaptic Localization of PKR and eIF2α. We found that PKR and its phosphorylated form are highly enriched at hippocampal and cortical synapses, indicating a compartmentalized distribution of the PKR-branch of the ISR in neurons. Previous studies have demonstrated the compartmentalization of the ISR in dividing cells (Zappa et al., 2022; Carrara et al., 2015; Kastan et al., 2020), discussed in (Boone and Zappa, 2023). For example, Zappa and colleagues (Zappa et al., 2022) recently described the localization of PKR to a granule membrane-less compartment in response to dsRNA, which excludes eIF2α and regulates downstream signaling. This prevents the interaction between PKR and eIF2α. Similarly, our observation of PKR distribution in Banker-cultured hippocampal neurons revealed clustering along axons (Fig. 4A). To our knowledge, this is the first description of an ISR protein compartmentalization in neurons.

In a study performed by Baleriola et al. (Baleriola et al., 2014), the local ISR activity in hippocampal neurons was examined. Although this study did not focus on the distribution of eIF2α or any of its kinases, it showed that under conditions of Aβ exposure, Atf4 mRNA is locally translated into axons, independent of the neuronal body, and associated with increased eIF2α phosphorylation. In our work, the co-localization of PKR with both presynaptic (Synapsin/Basson) and postsynaptic (PSD95) markers provides strong evidence for the PKR branch of the ISR's synaptic localization and supports its role in local synaptic processes. Furthermore, our findings also suggest that PKR activation modulates the degree of colocalization of eIF2α with presynaptic and postsynaptic markers (Fig. 8A, B). Together, these findings suggest that the ISR may modulate synaptic activity locally.

PKR Modulates Synaptic Protein Composition Size, and translation. Here, we demonstrate that the genetic ablation of PKR leads to a marked reduction in synaptic eIF2α phosphorylation and Synapsin levels, accompanied by significant alterations in synaptic architecture. Strikingly, these changes were confined to the hippocampus (Fig. 2A) and were not observed in cortical synapses (Fig. S7A), indicating a brain region-specific function of PKR in regulating synaptic composition. Notably, Synapsin levels decreased by more than 50 %, specifically at hippocampal synapses (Fig. 2A). Additionally, we found a reduction in Synapsin intensity at individual synapses in PKR-deficient mice (Fig. 9C). Synapsins are essential presynaptic proteins that tether synaptic vesicles (SVs) to the actin cytoskeleton, particularly within the reserve pool. Their phosphorylation state and abundance regulate the availability of SVs for release during neurotransmission (Cesca et al., 2010; Greengard et al., 1993). In the context of PKR deficiency, the decrease in Synapsin levels could significantly alter vesicle dynamics. Reduced Synapsin may lead to a loosening of vesicle tethering, thereby enhancing the mobilization of vesicles from the reserve pool to the readily releasable pool (Chi et al., 2003; Hilfiker et al., 2005). This shift could increase the number of vesicles available for immediate release upon stimulation, effectively raising the release probability at synapses. Moreover, the loss of Synapsin-mediated vesicle clustering could facilitate a more rapid replenishment of the releasable pool, especially during sustained activity. These effects could underlie the previously reported enhancements in synaptic efficacy and memory performance in

PKRKO animals. It is also possible that reduced Synapsin affects the spatial organization of vesicles and active zones, leading to a more permissive presynaptic architecture that favors neurotransmitter release (Pieribone et al., 1995; Milovanovic and De Camilli, 2017). These changes likely act in concert with other PKR-dependent modifications in synaptic composition to fine-tune presynaptic function. Thus, the reduction of Synapsin at synapses in PKRKO mice is likely to have profound effects on vesicle availability and release dynamics. This presynaptic reconfiguration may contribute directly to enhanced synaptic transmission and cognitive performance, linking structural remodeling with functional plasticity in the absence of PKR. Although our microscopy and biochemical data suggest potential functional consequences, direct evidence, such as electrophysiological measurements of synaptic activity or behavioral memory testing, will be essential in future studies to establish a causal link between the structural alterations and synaptic function.

Primary hippocampal neurons provide a powerful model for studying molecular and structural mechanisms with high resolution; however, they do not fully represent the complexity of the *in vivo* brain environment, where multiple cell types and circuit dynamics influence ISR signaling. Consequently, certain *in vitro* phenotypes—such as alterations in synaptic shape or the localization of ISR components—may not match those *in vivo*. However, our biochemical analyses of synaptoneurosomes from hippocampal and cortical tissue support the physiological presence and age-related regulation of PKR at synapses. Future research using *in vivo* or ultrastructural approaches in PKR-deficient models will be important to further validate and expand these findings.

The selective reduction of phosphorylated synaptic eIF2α observed in PKR-deficient mice (Fig. 2A, B) shows that PKR partially mediates synaptic eIF2α phosphorylation. This observation is particularly relevant considering the role of eIF2α phosphorylation in synaptic plasticity, learning, and memory (Sutton and Schuman, 2006; Di Prisco et al., 2014). eIF2α is essential for protein synthesis, and its phosphorylation induces a translational arrest but also allows the translation of specific mRNAs containing uORFs. uORFs-containing transcripts are part of the 800 mRNAs that are preferentially translated in the neuropil (axons, synapses, and dendrites) compared to somata (Glock et al., 2021). Thus, an active synaptic PKR, through eIF2α phosphorylation, could act as a proteostatic regulator and consequently change the composition in response to activity. So far, the synaptic localization of HRI, GCN2, or PERK, the other eIF2α kinases, has not been described. Here, we also observed the presence of PERK and GCN2 as proteins detectable at hippocampal synapses. If these kinases are active like PKR at synapses, they may also participate in synaptic eIF2α phosphorylation, as they have been implicated in memory and cognition (Costa-Mattioli et al., 2005; Sharma et al., 2018; G et al., 2013). However, in conditions of PKR deficiency, the reduction of nearly 70 % in phosphorylation levels suggests that PKR is the primary kinase involved in the phosphorylation of eIF2α. The reduction in eIF2α levels due to PKR deficiency was found only in hippocampal synapses (Fig. 2A, C) and not in cortical ones (Fig. S7A) and was not observed in the total hippocampal extracts (Fig. S5A). These results revealed a tissue-specific control of PKR over eIF2α levels and a compartmentalized control of the kinase over its substrate levels. Future studies are warranted to identify additional kinases or pathways that may modulate synaptic eIF2α activity and how these may be influenced by PKR loss in different physiological or pathological contexts. Interestingly, recent evidence has shown that GCN2 controls eIF2α levels in the brain after a demyelinating stimulus (Falcon et al., 2025). We propose that PKR is another ISR kinase controlling eIF2α levels in basal conditions and in a compartmentalized manner. Our measurements of *de novo* protein synthesis at the synapse showed increased levels in PKRKO-derived synaptic fractions. This result provides direct functional evidence that PKR acts as a local regulator of translation at the synapse. Mechanistically, this is consistent with our observation of decreased phosphorylated eIF2α levels at hippocampal synapses in PKR-deficient animals. Since phosphorylation of eIF2α is a well-established repressor of global protein synthesis, its reduction would relieve translational inhibition, thereby promoting local protein production. This suggests that the PKR-eIF2α signaling axis operates at synaptic compartments to dynamically regulate the local proteome.

Age-Related Changes in Synaptic PKR-eIF2α Signaling. PKR kinase and its target have been implicated in CNS aging and age-related diseases that affect cognitive abilities (Hussain and Ramaiah, 2007; Segev et al., 2013; Oliveira et al., 2021; Kim et al., 2007). In synapses derived from aged brains, we observed changes in synaptic composition characterized by increased PKR activation (phosphorylation) and a decrease in total eIF2α levels, without a corresponding increase in p-eIF2α, indicating an age-related shift in PKR-eIF2α signaling and suggesting that PKR may also influence local proteostasis through mechanisms that are partially independent of eIF2α phosphorylation. These findings, along with our results in PKR-deficient synapses, where we saw a reduction in puromycin incorporation, indicate that PKR regulates local translation at synapses and that age-related alterations in the balance between PKR activity and eIF2α availability could disrupt synaptic proteome homeostasis, potentially contributing to synaptic vulnerability and cognitive decline during aging and neurodegenerative processes. On the other hand, PKR activation has been associated with increased susceptibility to neurodegeneration, as it can exacerbate neuroinflammation and cognitive decline (Cheng et al., 2025; Trinh and Klann, 2013). Moreover, activated PKR has been found in the context of age-dependent neurodegenerative diseases, particularly in Alzheimer's Disease patients and mouse models (Peel and Bredesen, 2003). In addition to its role in the integrated stress response, PKR is also a key effector downstream of type I interferon signaling, where it is transcriptionally induced and activated by double-stranded RNA during antiviral responses (Martinez et al., 2021). This pathway is increasingly recognized as being abnormally activated in the aging brain and in various neurodegenerative diseases, where chronic neuroinflammation and dysregulated interferon responses are prominent features. In this context, the increased synaptic phosphorylation of PKR observed in aged brains may not only reflect intrinsic stress responses but could also result from enhanced interferon signaling. This raises the possibility that immune-related pathways may influence synaptic PKR activity and, by extension, affect local translation and synaptic integrity. Therefore, our findings may have implications that extend beyond stress responses, potentially linking synaptic changes to neuroimmune mechanisms in the context of aging and disease. Future studies exploring the intersection of interferon signaling, PKR activation, and synaptic function could provide valuable insights into how neuroinflammation contributes to cognitive decline. Overall, our results revealed an alteration of the PKR-eIF2α axis at synapses in aged synapses. It remains to be established whether the activated synaptic PKR contributes, in part, to the synaptic dysfunction and cognitive decline in aging.

Our results show that synaptic-enriched fractions from 9 to 12-month animals are associated with reduced levels of PSD95 and Synapsin, which align with previously described findings (VanGuilder et al., 2010; VanGuilder et al., 2011). This age range, which corresponds to a middle-aged stage in mice rather than advanced aging, shows early molecular and structural alterations in the brain that precede overt behavioral or neurodegenerative phenotypes. For instance, changes in hippocampal long-term potentiation (LTP) and reductions in field excitatory post-synaptic potential (fEPSP) amplitudes have been observed by 9 months of age (Pereda et al., 2019). Similarly, modifications in synaptic vesicle pool organization (Nikonenko and Skibo, 2025) and altered expression of synaptic proteins involved in neurotransmission and plasticity have been reported in the hippocampus within this time frame (VanGuilder et al., 2010). Importantly, signs of cognitive decline, particularly in spatial learning and memory, have also been detected in 12-month-old mice (Li et al., 2020). In aged synapses, we found decreased synaptic eIF2α levels without changes in cytosolic levels (Fig. 1C, D). These results indicate that the mechanism maintaining eIF2α at the synapse

could be altered during this early stage of aging. Based on the opposite results in cortical synapses, this mechanism is differentially affected across brain regions. Associated with aging, increased PKR activation was found only in hippocampal synapses. Intriguingly, this profound increase in synaptic PKR activation (phosphorylation) was not correlated with increased eIF2α phosphorylation levels at the synapses. This could be related to PKR's kinase activity being negatively regulated during aging, as described by Hussain and Ramaiah (Hussain and Ramaiah, 2007). They described that total brain cortical extracts derived from aged mice negatively affect the kinase activity of a recombinant PKR protein. It remains to be determined that it is also extensible to hippocampal synapses. Overall, our results revealed an alteration of the PKR-eIF2α axis at synapses in aged synapses.

Together, our results support a novel role for PKR as a controller of synaptic structural plasticity, highlighting the integrated stress response as a spatially organized signaling pathway that can directly shape synaptic composition and function. Dysregulation of the axis PKR-eIF2α may contribute to region-specific synaptic vulnerability during aging.

Broader Implications and Future Directions. Our study highlights the importance of synaptic PKR signaling in regulating synaptic proteins, aging, ISR activation, and translation. The presence of dynamic PKR and eIF2α at synapses suggests that local ISR regulation is crucial for synaptic function, while age-related alterations in this pathway may contribute to synaptic decline and cognitive impairments. Future studies should investigate the molecular mechanisms underlying PKR-mediated synaptic ISR activation, including interactions with other ISR kinases such as GCN2 and PERK. Additionally, exploring how PKR modulation affects synaptic plasticity and behavior in aging and disease models could provide valuable insights into the therapeutic potential of ISR-targeting strategies. Overall, our findings establish a novel role for PKR-eIF2α signaling at synapses and lay the groundwork for future research into synaptic ISR dynamics and their relevance to CNS physiology, aging, and disease.

Credit authorship contribution statement

Nicolás W. Martínez: Writing – review & editing, Writing – original draft, Investigation, Funding acquisition, Formal analysis, Conceptualization. **Felipe Gómez:** Writing – review & editing, Writing – original draft, Investigation, Formal analysis. **Ariel Tapia-Godoy:** Investigation. **Juan Francisco Roa:** Investigation. **Fernanda Moreso-Contreras:** Investigation. **Yuwei Liu:** Investigation. **Claudia Jara:** Investigation. **Cheril Tapia-Rojas:** Investigation, Funding acquisition. **Iván Alfaro:** Supervision, Funding acquisition, Conceptualization. **Mauro Costa-Mattioli:** Writing – review & editing, Funding acquisition. **Soledad Matus:** Writing – review & editing, Writing – original draft, Supervision, Project administration, Funding acquisition.

Ethics approval

All the studies were conducted according to the eighth edition of the Guide for the Care and Use of Laboratory Animals. The experimental protocols, including those involving anesthesia, pain, distress, and euthanasia (No P014/2020, the ethical approval date was May 8, 2020), were approved by the IACUC at the FCV.

Funding

This work was supported by the National Agency of Research and Development (ANID): "Financiamiento Basal para Centros Científicos y Tecnológicos de Excelencia Centro Ciencia & Vida" ANID BASAL FB210008 (S.M., C.T.R.); FONDECYT ANID 1230334 (S.M.) and FONDECYT ANID 1221178 (C.T.R); FONDECYT Postdoc ANID 3200932 (N. W.M.); FONDAP/15150012 (S.M.); ANID FONDEQUIP - EQY230019 (I. A.).

Declaration of competing interest

N.W.M., F.G., A.T.G., J.F.R., F.M.C., I.A., C.J., C.T.R., and S.M. declare that they have no competing interests. M.C.M. and Y.L. are employed by Altos Labs.

Acknowledgments

We thank the animal facility at FCV/Universidad San Sebastián, the "Unidad de Microscopia Avanzada" (UMA) at Pontificia Universidad Católica, Santiago, Chile, for the electron microscopy work and the Microscopy Facility REDECA at Universidad de Chile.

Appendix A. Supplementary data

Supplementary data to this article can be found online at https://doi.org/10.1016/j.nbd.2025.107113.

Data availability

The datasets used and/or analyzed during this current study are available from the corresponding author upon reasonable request.

References

Alvarez, J., 2001. The autonomous axon: a model based on local synthesis of proteins. Biol. Res. 34 (2), 103–109.
Alvarez, J., Giuditta, A., Koenig, E., 2000. Protein synthesis in axons and terminals: significance for maintenance, plasticity and regulation of phenotype. With a critique of slow transport theory. Prog. Neurobiol. 62 (1), 1–62.
Alvarez-Castelao, B., et al., 2020. The switch-like expression of heme-regulated kinase 1 mediates neuronal proteostasis following proteasome inhibition. Elife 9.
Anderson, E., et al., 2011. Heparin activates PKR by inducing dimerization. J. Mol. Biol. 413 (5), 973–984.
Azpurua, J., Eaton, B.A., 2015. Neuronal epigenetics and the aging synapse. Front. Cell. Neurosci. 9, 208.
Baleriola, J., et al., 2014. Axonally synthesized ATF4 transmits a neurodegenerative signal across brain regions. Cell 158 (5), 1159–1172.
Banker, G.A., Cowan, W.M., 1979. Further observations on hippocampal neurons in dispersed cell culture. J. Comp. Neurol. 187 (3), 469–493.
Barragan-Iglesias, P., et al., 2020. Type I interferons act directly on nociceptors to produce pain sensitization: implications for viral infection-induced pain. J. Neurosci. 40 (18), 3517–3532.
Barrantes, F.J., 2024. Cognitive synaptopathy: synaptic and dendritic spine dysfunction in age-related cognitive disorders. Front. Aging Neurosci. 16, 1476909.
Batista, G., et al., 2016. Translational control of auditory imprinting and structural plasticity by eIF2alpha. Elife 5.
Benson, D.L., et al., 1994. Characterization of GABAergic neurons in hippocampal cell cultures. J. Neurocytol. 23 (5), 279–295.
Bernsen, J., 1986. Dynamic thresholding of gray-level images. In: Proc. Eighth Int'l Conf. Pattern Recognition, Paris, p. 1986.
Biever, A., et al., 2016. Repeated exposure to D-amphetamine decreases global protein synthesis and regulates the translation of a subset of mRNAs in the striatum. Front. Mol. Neurosci. 9, 165.
Bin Ibrahim, M.Z., Benoy, A., Sajikumar, S., 2022. Long-term plasticity in the hippocampus: maintaining within and 'tagging' between synapses. FEBS J. 289 (8), 2176–2201.
Bolte, S., Cordelières, F.P., 2006. A guided tour into subcellular colocalization analysis in light microscopy. J. Microsc. 224 (Pt 3), 213–232.
Boone, M., Zappa, F., 2023. Signaling plasticity in the integrated stress response. Front. Cell Dev. Biol. 11, 1271141.
Carrara, M., et al., 2015. Crystal structures reveal transient PERK luminal domain tetramerization in endoplasmic reticulum stress signaling. EMBO J. 34 (11), 1589–1600.
Caterino, C., et al., 2024. The aging synapse: an integrated proteomic and transcriptomic analysis. bioRxiv preprint 1–39. https://doi.org/10.1101/2024.12.18.629115.
Cesca, F., et al., 2010. The synapsins: key actors of synapse function and plasticity. Prog. Neurobiol. 91 (4), 313–348.
Chang, R.C., et al., 2002. Phosphorylation of eukaryotic initiation factor-2alpha (eIF2alpha) is associated with neuronal degeneration in Alzheimer's disease. Neuroreport 13 (18), 2429–2432.
Cheng, W.Y., et al., 2025. PKR modulates sterile systemic inflammation-triggered neuroinflammation and brain glucose metabolism disturbances. Front. Immunol. 16, 1469737.
Chi, P., Greengard, P., Ryan, T.A., 2003. Synaptic vesicle mobilization is regulated by distinct synapsin I phosphorylation pathways at different frequencies. Neuron 38 (1), 69–78.

Cicali, K.A., Tapia-Rojas, C., 2024. Synaptic mitochondria: a crucial factor in the aged hippocampus. Ageing Res. Rev. 101, 102524.
Costa-Mattioli, M., Walter, P., 2020. The integrated stress response: from mechanism to disease. Science 368 (6489).
Costa-Mattioli, M., et al., 2005. Translational control of hippocampal synaptic plasticity and memory by the eIF2alpha kinase GCN2. Nature 436 (7054), 1166–1173.
Costa-Mattioli, M., et al., 2007. eIF2alpha phosphorylation bidirectionally regulates the switch from short- to long-term synaptic plasticity and memory. Cell 129 (1), 195–206.
Court, F.A., Alvarez, J., 2005. Local regulation of the axonal phenotype, a case of merotrophism. Biol. Res. 38 (4), 365–374.
Court, F.A., et al., 2008. Schwann cell to axon transfer of ribosomes: toward a novel understanding of the role of glia in the nervous system. J. Neurosci. 28 (43), 11024–11029.
Davis, G.A., Bloom, F.E., 1973. Isolation of synaptic junctional complexes from rat brain. Brain Res. 62 (1), 135–153.
Deb, A., et al., 2001. Protein kinase PKR is required for platelet-derived growth factor signaling of c-fos gene expression via Erks and Stat3. EMBO J. 20 (10), 2487–2496.
Derisbourg, M.J., Hartman, M.D., Denzel, M.S., 2021a. Perspective: modulating the integrated stress response to slow aging and ameliorate age-related pathology. Nat. Aging 1 (9), 760–768.
Derisbourg, M.J., et al., 2021b. Mutagenesis screen uncovers lifespan extension through integrated stress response inhibition without reduced mRNA translation. Nat. Commun. 12 (1), 1678.
Derisbourg, M.J., Wester, L.E., Baddi, R., et al., 2021. Mutagenesis screen uncovers lifespan extension through integrated stress response inhibition without reduced mRNA translation. Nat. Commun. 12, 1678. https://doi.org/10.1038/s41467-021-21743-x.
Dey, M., et al., 2005. Mechanistic link between PKR dimerization, autophosphorylation, and eIF2alpha substrate recognition. Cell 122 (6), 901–913.
Di Prisco, G.V., et al., 2014. Translational control of mGluR-dependent long-term depression and object-place learning by eIF2alpha. Nat. Neurosci. 17 (8), 1073–1082.
Dong, C., et al., 2008. Proteasome inhibition enhances the induction and impairs the maintenance of late-phase long-term potentiation. Learn. Mem. 15 (5), 335–347.
Dorrbaum, A.R., et al., 2018. Local and global influences on protein turnover in neurons and glia. Elife 7.
Dorrbaum, A.R., et al., 2020. Proteome dynamics during homeostatic scaling in cultured neurons. Elife 9.
Dunn, K.W., Kamocka, M.M., McDonald, J.H., 2011. A practical guide to evaluating colocalization in biological microscopy. Am. J. Phys. Cell Phys. 300 (4), C723–C742.
Falcon, P., et al., 2025. GCN2-mediated eIF2alpha phosphorylation is required for central nervous system remyelination. Int. J. Mol. Sci. 26 (4).
Fan, W.J., et al., 2018. Synaptic aging disrupts synaptic morphology and function in cerebellar Purkinje cells. Neural Regen. Res. 13 (6), 1019–1025.
Farías, G.G., et al., 2009. Wnt-5a/JNK signaling promotes the clustering of PSD-95 in hippocampal neurons. J. Biol. Chem. 284 (23), 15857–15866.
G, I.L.-R., et al., 2013. Consolidation of object recognition memory requires HRI kinase-dependent phosphorylation of eIF2alpha in the hippocampus. Hippocampus 23 (6), 431–436.
Garcia, M.A., Meurs, E.F., Esteban, M., 2007. The dsRNA protein kinase PKR: virus and cell control. Biochimie 89 (6–7), 799–811.
Giandomenico, S.L., Alvarez-Castelao, B., Schuman, E.M., 2022. Proteostatic regulation in neuronal compartments. Trends Neurosci. 45 (1), 41–52.
Glock, C., et al., 2021. The translatome of neuronal cell bodies, dendrites, and axons. Proc. Natl. Acad. Sci. USA 118 (43).
Graham, L.C., et al., 2021. Temporal profiling of the cortical synaptic mitochondrial proteome identifies ageing associated regulators of stability. Cells 10 (12).
Greengard, P., et al., 1993. Synaptic vesicle phosphoproteins and regulation of synaptic function. Science 259 (5096), 780–785.
Gumy, L.F., Tan, C.L., Fawcett, J.W., 2010. The role of local protein synthesis and degradation in axon regeneration. Exp. Neurol. 223 (1), 28–37.
Hafner, A.S., et al., 2019. Local protein synthesis is a ubiquitous feature of neuronal pre- and postsynaptic compartments. Science 364 (6441).
Harding, H.P., et al., 2000. Regulated translation initiation controls stress-induced gene expression in mammalian cells. Mol. Cell 6 (5), 1099–1108.
He, Y., Franchi, L., Nunez, G., 2013. The protein kinase PKR is critical for LPS-induced iNOS production but dispensable for inflammasome activation in macrophages. Eur. J. Immunol. 43 (5), 1147–1152.
Hegde, A.N., 2004. Ubiquitin-proteasome-mediated local protein degradation and synaptic plasticity. Prog. Neurobiol. 73 (5), 311–357.
Hegde, A.N., et al., 2014. Local ubiquitin-proteasome-mediated proteolysis and long-term synaptic plasticity. Front. Mol. Neurosci. 7, 96.
Hilfiker, S., et al., 2005. Structural domains involved in the regulation of transmitter release by synapsins. J. Neurosci. 25 (10), 2658–2669.
Hinnebusch, A.G., 2005. Translational regulation of GCN4 and the general amino acid control of yeast. Ann. Rev. Microbiol. 59, 407–450.
Hobson, B.D., et al., 2022. Subcellular proteomics of dopamine neurons in the mouse brain. Elife 11.
Hoozemans, J.J., et al., 2007. Activation of the unfolded protein response in Parkinson's disease. Biochem. Biophys. Res. Commun. 354 (3), 707–711.
Husain, B., Hesler, S., Cole, J.L., 2015. Regulation of PKR by RNA: formation of active and inactive dimers. Biochemistry 54 (44), 6663–6672.
Hussain, S.G., Ramaiah, K.V., 2007. Reduced eIF2alpha phosphorylation and increased proapoptotic proteins in aging. Biochem. Biophys. Res. Commun. 355 (2), 365–370.
Hwang, K.D., et al., 2017. Restoring synaptic plasticity and memory in mouse models of Alzheimer's disease by PKR inhibition. Mol. Brain 10 (1), 57.
Jedrzejewska-Szmek, J., Blackwell, K.T., 2019. From membrane receptors to protein synthesis and actin cytoskeleton: mechanisms underlying long lasting forms of synaptic plasticity. Semin. Cell Dev. Biol. 95, 120–129.
Jiang, Z., et al., 2010. eIF2alpha phosphorylation-dependent translation in CA1 pyramidal cells impairs hippocampal memory consolidation without affecting general translation. J. Neurosci. 30 (7), 2582–2594.
Jung, H., Yoon, B.C., Holt, C.E., 2012. Axonal mRNA localization and local protein synthesis in nervous system assembly, maintenance and repair. Nat. Rev. Neurosci. 13 (5), 308–324.
Kaech, S., Banker, G., 2006. Culturing hippocampal neurons. Nat. Protoc. 1 (5), 2406–2415.
Kang, H., Schuman, E.M., 1996. A requirement for local protein synthesis in neurotrophin-induced hippocampal synaptic plasticity. Science 273 (5280), 1402–1406.
Kastan, J.P., et al., 2020. CReP mediates selective translation initiation at the endoplasmic reticulum. Sci. Adv. 6 (23), eaba0745.
Kim, E., Jung, H., 2015. Local protein synthesis in neuronal axons: why and how we study. BMB Rep. 48 (3), 139–146.
Kim, H.S., et al., 2007. Swedish amyloid precursor protein mutation increases phosphorylation of eIF2alpha in vitro and in vivo. J. Neurosci. Res. 85 (7), 1528–1537.
Kim, Y., et al., 2018. PKR senses nuclear and mitochondrial signals by interacting with endogenous double-stranded RNAs. Mol. Cell 71 (6), 1051–1063 e6.
Krukowski, K., et al., 2020. Small molecule cognitive enhancer reverses age-related memory decline in mice. Elife 9.
Lacor, P.N., et al., 2007. Abeta oligomer-induced aberrations in synapse composition, shape, and density provide a molecular basis for loss of connectivity in Alzheimer's disease. J. Neurosci. 27 (4), 796–807.
Ladiges, W., et al., 2000. Tissue specific expression of PKR protein kinase in aging B6D2F1 mice. Mech. Ageing Dev. 114 (2), 123–132.
Li, Q., et al., 2004a. A Syntaxin 1, $G\alpha_o$, and N-type calcium channel complex at a presynaptic nerve terminal: analysis by quantitative immunocolocalization. J. Neurosci. 24 (16), 4070–4081.
Li, Q., et al., 2004b. A syntaxin 1, Galpha(o), and N-type calcium channel complex at a presynaptic nerve terminal: analysis by quantitative immunocolocalization. J. Neurosci. 24 (16), 4070–4081.
Li, M., et al., 2020. Differentially expressed genes in the brain of aging mice with cognitive alteration and depression- and anxiety-like behaviors. Front. Cell Dev. Biol. 8, 814.
Li, F., et al., 2024. Morphological correlates of synaptic protein turnover in the mouse brain. Life Sci. Alliance 7 (11).
Liu, J., et al., 2014. Activating transcription factor 4 (ATF4) modulates post-synaptic development and dendritic spine morphology. Front. Cell. Neurosci. 8, 177.
Lockshin, E.R., Calakos, N., 2024. The integrated stress response in brain diseases: a double-edged sword for proteostasis and synapses. Curr. Opin. Neurobiol. 87, 102886.
Lourenco, M.V., et al., 2013. TNF-alpha mediates PKR-dependent memory impairment and brain IRS-1 inhibition induced by Alzheimer's beta-amyloid oligomers in mice and monkeys. Cell Metab. 18 (6), 831–843.
Lu, P.D., Harding, H.P., Ron, D., 2004. Translation reinitiation at alternative open reading frames regulates gene expression in an integrated stress response. J. Cell Biol. 167 (1), 27–33.
Maiellano, G., Scandella, L., Francolini, M., 2023. Exploiting volume electron microscopy to investigate structural plasticity and stability of the postsynaptic compartment of central synapses. Front. Cell. Neurosci. 17, 1153593.
Martinez, N.W., Gomez, F.E., Matus, S., 2021. The potential role of protein kinase R as a regulator of age-related neurodegeneration. Front. Aging Neurosci. 13, 638208.
McAllister, C.S., Taghavi, N., Samuel, C.E., 2012. Protein kinase PKR amplification of interferon beta induction occurs through initiation factor eIF-2alpha-mediated translational control. J. Biol. Chem. 287 (43), 36384–36392.
Michaelis, M.L., Jiang, L., Michaelis, E.K., 2017. Isolation of synaptosomes, synaptic plasma membranes, and synaptic junctional complexes. Methods Mol. Biol. 1538, 107–119.
Milovanovic, D., De Camilli, P., 2017. Synaptic vesicle clusters at synapses: a distinct liquid phase? Neuron 93 (5), 995–1002.
Moon, S.L., Sonenberg, N., Parker, R., 2018. Neuronal regulation of eIF2alpha function in health and neurological disorders. Trends Mol. Med. 24 (6), 575–589.
Murai, Y., Goto, A., 2025. Diverse synaptic mechanisms underlying learning and memory consolidation. Curr. Opin. Neurobiol. 92, 102996.
Navakkode, S., Kennedy, B.K., 2024. Neural ageing and synaptic plasticity: prioritizing brain health in healthy longevity. Front. Aging Neurosci. 16, 1428244.
Nguyen, P.V., Abel, T., Kandel, E.R., 1994. Requirement of a critical period of transcription for induction of a late phase of LTP. Science 265 (5175), 1104–1107.
Nikonenko, A.G., Skibo, G.G., 2025. Age-related changes in synaptic vesicle pools of axo-dendritic synapses on hippocampal CA1 pyramidal neurons in mice.
Oliveira, M.M., et al., 2021. Correction of eIF2-dependent defects in brain protein synthesis, synaptic plasticity, and memory in mouse models of Alzheimer's disease. Sci. Signal. 14 (668).
Page, G., et al., 2006. Activated double-stranded RNA-dependent protein kinase and neuronal death in models of Alzheimer's disease. Neuroscience 139 (4), 1343–1354.
Peel, A.L., Bredesen, D.E., 2003. Activation of the cell stress kinase PKR in Alzheimer's disease and human amyloid precursor protein transgenic mice. Neurobiol. Dis. 14 (1), 52–62.

Pereda, D., et al., 2019. Changes in presynaptic calcium signalling accompany age-related deficits in hippocampal LTP and cognitive impairment. Aging Cell 18 (5), e13008.
Pertz, O.C., et al., 2008. Spatial mapping of the neurite and soma proteomes reveals a functional Cdc42/Rac regulatory network. Proc. Natl. Acad. Sci. USA 105 (6), 1931–1936.
Petralia, R.S., Mattson, M.P., Yao, P.J., 2014. Communication breakdown: the impact of ageing on synapse structure. Ageing Res. Rev. 14, 31–42.
Pieribone, V.A., et al., 1995. Distinct pools of synaptic vesicles in neurotransmitter release. Nature 375 (6531), 493–497.
Placzek, A.N., et al., 2016. eIF2alpha-mediated translational control regulates the persistence of cocaine-induced LTP in midbrain dopamine neurons. Elife 5.
Rajgor, D., Welle, T.M., Smith, K.R., 2021. The coordination of local translation, membranous organelle trafficking, and synaptic plasticity in neurons. Front. Cell Dev. Biol. 9, 711446.
Ramasamy, V.S., et al., 2025. Abeta(42) induces stress granule formation via PACT/PKR pathway. Sci. Rep. 15 (1), 5829.
Reimer, L., et al., 2018. Inflammation kinase PKR phosphorylates alpha-synuclein and causes alpha-synuclein-dependent cell death. Neurobiol. Dis. 115, 17–28.
Romano, P.R., et al., 1998. Autophosphorylation in the activation loop is required for full kinase activity in vivo of human and yeast eukaryotic initiation factor 2alpha kinases PKR and GCN2. Mol. Cell. Biol. 18 (4), 2282–2297.
Roque, P.J., Guizzetti, M., Costa, L.G., 2014. Synaptic structure quantification in cultured neurons. Curr. Protoc. Toxicol. 60, p. 12 22 1-32.
Scarim, A.L., et al., 2001. Mechanisms of beta-cell death in response to double-stranded (ds) RNA and interferon-gamma: dsRNA-dependent protein kinase apoptosis and nitric oxide-dependent necrosis. Am. J. Pathol. 159 (1), 273–283.
Schikorski, T., Stevens, C.F., 1997. Quantitative ultrastructural analysis of hippocampal excitatory synapses. J. Neurosci. 17 (15), 5858–5867.
Schindelin, J., et al., 2012. Fiji: an open-source platform for biological-image analysis. Nat. Methods 9 (7), 676–682.
Schneider, C.A., Rasband, W.S., Eliceiri, K.W., 2012. NIH image to ImageJ: 25 years of image analysis. Nat. Methods 9 (7), 671–675.
Segev, Y., Michaelson, D.M., Rosenblum, K., 2013. ApoE epsilon4 is associated with eIF2alpha phosphorylation and impaired learning in young mice. Neurobiol. Aging 34 (3), 863–872.
Segref, A., Hoppe, T., 2009. Think locally: control of ubiquitin-dependent protein degradation in neurons. EMBO Rep. 10 (1), 44–50.
Sharma, V., et al., 2018. Local inhibition of PERK enhances memory and reverses age-related deterioration of cognitive and neuronal properties. J. Neurosci. 38 (3), 648–658.
Shrestha, P., et al., 2020. Cell-type-specific drug-inducible protein synthesis inhibition demonstrates that memory consolidation requires rapid neuronal translation. Nat. Neurosci. 23 (2), 281–292.
Smith, H.L., Mallucci, G.R., 2016. The unfolded protein response: mechanisms and therapy of neurodegeneration. Brain 139 (Pt 8), 2113–2121.
Sotelo, J.R., et al., 2014. Glia to axon RNA transfer. Dev. Neurobiol. 74 (3), 292–302.
Spaulding, E.L., Burgess, R.W., 2017. Accumulating evidence for axonal translation in neuronal homeostasis. Front. Neurosci. 11, 312.
Stauch, K.L., Purnell, P.R., Fox, H.S., 2014. Aging synaptic mitochondria exhibit dynamic proteomic changes while maintaining bioenergetic function. Aging (Albany NY) 6 (4), 320–334.
Stern, E., et al., 2013. Blocking the eIF2alpha kinase (PKR) enhances positive and negative forms of cortex-dependent taste memory. J. Neurosci. 33 (6), 2517–2525.
Steward, O., Schuman, E.M., 2001. Protein synthesis at synaptic sites on dendrites. Annu. Rev. Neurosci. 24, 299–325.
Sutton, M.A., Schuman, E.M., 2006. Dendritic protein synthesis, synaptic plasticity, and memory. Cell 127 (1), 49–58.
Takizawa, T., et al., 2000. Three leucine-rich sequences and the N-terminal region of double-stranded RNA-activated protein kinase (PKR) are responsible for its cytoplasmic localization. J. Biochem. 128 (3), 471–476.
Trinh, M.A., Klann, E., 2013. Translational control by eIF2alpha kinases in long-lasting synaptic plasticity and long-term memory. Neurobiol. Learn. Mem. 105, 93–99.
Tu, W.Y., et al., 2024. Local protein synthesis at neuromuscular synapses is required for motor functions. Cell Rep. 43 (9), 114661.
Upadhya, S.C., et al., 2006. Differential regulation of proteasome activity in the nucleus and the synaptic terminals. Neurochem. Int. 48 (4), 296–305.
van Steensel, B., et al., 1996. Partial colocalization of glucocorticoid and mineralocorticoid receptors in discrete compartments in nuclei of rat hippocampus neurons. J. Cell Sci. 109 (Pt 4), 787–792.
VanGuilder, H.D., et al., 2010. Aging alters the expression of neurotransmission-regulating proteins in the hippocampal synaptoproteome. J. Neurochem. 113 (6), 1577–1588.
VanGuilder, H.D., et al., 2011. Hippocampal dysregulation of synaptic plasticity-associated proteins with age-related cognitive decline. Neurobiol. Dis. 43 (1), 201–212.
Vattem, K.M., Wek, R.C., 2004. Reinitiation involving upstream ORFs regulates ATF4 mRNA translation in mammalian cells. Proc. Natl. Acad. Sci. USA 101 (31), 11269–11274.
Vegh, M.J., et al., 2014. Hippocampal extracellular matrix levels and stochasticity in synaptic protein expression increase with age and are associated with age-dependent cognitive decline. Mol. Cell. Proteomics 13 (11), 2975–2985.
Wek, R.C., 2018. Role of eIF2alpha kinases in translational control and adaptation to cellular stress. Cold Spring Harb. Perspect. Biol. 10 (7).
Wek, R.C., Jiang, H.Y., Anthony, T.G., 2006. Coping with stress: eIF2 kinases and translational control. Biochem. Soc. Trans. 34 (Pt 1), 7–11.
Yang, Y.L., et al., 1995. Deficient signaling in mice devoid of double-stranded RNA-dependent protein kinase. EMBO J. 14 (24), 6095–6106.
Zappa, F., et al., 2022. Signaling by the integrated stress response kinase PKR is fine-tuned by dynamic clustering. J. Cell Biol. 221 (7).
Zhu, P.J., et al., 2011. Suppression of PKR promotes network excitability and enhanced cognition by interferon-gamma-mediated disinhibition. Cell 147 (6), 1384–1396.